

UNCLASSIFIED

AD 277 642

*Reproduced
by the*

**ARMED SERVICES TECHNICAL INFORMATION AGENCY
ARLINGTON HALL STATION
ARLINGTON 12, VIRGINIA**



UNCLASSIFIED

NOTICE: When government or other drawings, specifications or other data are used for any purpose other than in connection with a definitely related government procurement operation, the U. S. Government thereby incurs no responsibility, nor any obligation whatsoever; and the fact that the Government may have formulated, furnished, or in any way supplied the said drawings, specifications, or other data is not to be regarded by implication or otherwise as in any manner licensing the holder or any other person or corporation, or conveying any rights or permission to manufacture, use or sell any patented invention that may in any way be related thereto.

CATALOGED BY ASTIA 277642
AS AD No

ASD-TR-61-657

277 642

**RESEARCH ON ELECTRON BOMBARDMENT INDUCED
CONDUCTIVITY TARGETS IN CAMERA TUBES**

TECHNICAL REPORT No. ASD-TR-61-657

APRIL 1962

ELECTRONIC TECHNOLOGY LABORATORY
AERONAUTICAL SYSTEMS DIVISION
AIR FORCE SYSTEMS COMMAND
WRIGHT-PATTERSON AIR FORCE BASE, OHIO

Project No. 4156, Task No. 415605

ASTIA
RECEIVED
JUL 12 1962
11-67-4-2
TISIA

(Prepared under Contract No. AF 33(616)-6496
by Westinghouse Research Lab., Pittsburgh, Pa.
Authors: J. Lempert and G. Klotzbaugh)

NOTICES

When Government drawings, specifications, or other data are used for any purpose other than in connection with a definitely related Government procurement operation, the United States Government thereby incurs no responsibility nor any obligation whatsoever; and the fact that the Government may have formulated, furnished, or in any way supplied the said drawings, specifications, or other data, is not to be regarded by implication or otherwise as in any manner licensing the holder or any other person or corporation, or conveying any rights or permission to manufacture, use, or sell any patented invention that may in any way be related thereto.

Qualified requesters may obtain copies of this report from the Armed Services Technical Information Agency, (ASTIA), Arlington Hall Station, Arlington 12, Virginia.

This report has been released to the Office of Technical Services, U.S. Department of Commerce, Washington 25, D.C., in stock quantities for sale to the general public.

Copies of this report should not be returned to the Aeronautical Systems Division unless return is required by security considerations, contractual obligations, or notice on a specific document.

FOREWORD

This report was prepared by Westinghouse Research Laboratories, Pittsburgh, Pennsylvania, on Air Force Contract AF 33(616)-6496, under Task No. 415605 of Project No. 4156, "Electronic Tube Technology". The work was administered under the direction of Electronic Technology Laboratory, Aeronautical Systems Division. Mr. Melvin R. St. John was Project Engineer for the Laboratory.

The studies presented began in May 1959 and this report describes the research performed during the period from October 1960 through October 1961.

The experimental tubes built on this program were fabricated under the supervision of Mr. A. Crans and Mr. D. Doughty, and evaluated by Dr. G. Klotzbaugh. Mr. J. Lempert was responsible for the target program and served as principal investigator.

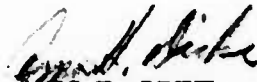
ABSTRACT

An analysis of scan parameters as they affect the performance of electron bombardment induced conductivity (EBIC) targets is presented. The conclusion is reached that the secondary emission characteristic of the target surface is an extremely important parameter in camera tubes of the photoconductivity and EBIC types. Evidence that the electron absorptivity of the target for low voltage electrons is affected by the degree of induced excitation is presented. Results of an investigation of different EBIC target materials are reviewed. The fabrication of experimental EBIC tubes having electrostatic and magnetic focused image sections is described. Test results to date are discussed.

PUBLICATION REVIEW

The publication of this report does not constitute approval by the Air Force of the findings or conclusions contained herein. It is published only for the exchange and stimulation of ideas.

FOR THE COMMANDER:



AMOS H. DICKE
Chief, Thermionics Branch
Electronic Technology Laboratory

TABLE OF CONTENTS

	Page
1) Introduction.	1
2) Army Signal Corps Program	3
3) Investigation of Scan Parameters as They Affect Target Performance.	4
a. Simplified Theory of Target Scan.	4
b. Experimental Investigation of Target Scan Parameters.	19
c. Discussion of Electron Absorptivity of Insulators	38
4) Survey of EBIC Target Materials	43
a. Arsenic Compounds of the $M_2^{VB}X^{VIB}$ Family.	43
b. Ternary Formulations Incorporating As and Se.	45
c. Summary of Sb_2S_3 Type Materials	49
d. Alkali Halides.	52
e. Miscellaneous Materials	52
1. $Cd_3As_3Se_6As_2O_3$	52
2. GaP , Al_2Te_3 and Ga_2Se_3	52
5) Tube Program.	52
a. Introduction.	52
b. Tube E-I.	52
c. Tube E-II	54
d. Tube E-III.	57
e. Tube E-IV	59
6) Conclusions	60
List of References.	62

LIST OF FIGURES

Figure	Page
1 - EBIC target scan parameters assuming target resistance $R = 10^9$ ohms and $\bar{\delta} = 1 - 1.7 \times 10^{-2} \bar{V}_S + 2.8 \times 10^{-4} \bar{V}_S^2$; for indicated values of I_B	10
2 - EBIC target scan parameters for $\bar{\delta} = 1 - 1.7 \times 10^{-2} \bar{V}_S + 2.8 \times 10^{-4} \bar{V}_S^2$, the indicated values of target resistance in ohms and $I_B = 3 \times 10^{-7}$ A	12
3 - As function of \bar{V}_S : Target leakage currents for different values of target resistance; also beam landing signal $I_B(1-\bar{\delta})$ for different values of I_B	14
4 - Target signal current as function of beam current for various values of target resistance. Assumes $V_T = 50$ volts and $\bar{\delta} = 1 - 1.7 \times 10^{-2} \bar{V}_S + 2.8 \times 10^{-4} \bar{V}_S^2$	16
5 - Target surface potentials as function of beam current for parameters of Fig. 7	17
6 - EBIC signal current for As_2S_2 target as function of input current (target 581 ARL, $V_T = 50$ volts)	21
7 - Resistance of As_2S_3 and As_2S_2 EBIC targets as function of input current	22
8 - Plot of $(1-\bar{\delta})$ as function of \bar{V}_S for As_2S_2 target (target 581 ARL, $V_T = 50$ volts)	24
9 - Target surface potential \bar{V}_S as function of input current for As_2S_2 target and different values of beam current	25
10 - Plot of $(1-\bar{\delta})$ under imaging conditions as function of \bar{V}_S for As_2S_2 target	26
11 - EBIC signal current for As_2S_2 target as function of I_B for different values of input current	27
12 - Plot of $(1-\bar{\delta})$ under imaging conditions as function of \bar{V}_S for As_2S_2 target	28
13 - Plot of $(1-\bar{\delta})$ under imaging conditions as function of \bar{V}_S for As_2S_2 target after overnight exposure in demountable	29
14 - Plot of $1-\bar{\delta}$ as function of \bar{V}_S for As_2S_3 targets	31
15 - Plot of $(1-\bar{\delta})$ as function of \bar{V}_S for EBIC targets with vacuum evaporated overlayer of Sb_2S_3	32
16 - Plot of $(1-\bar{\delta})$ as function of \bar{V}_S for As_2S_2 with Sb_2S_3 vacuum evaporated overlayer	33
17 - Plot of $(1-\bar{\delta})$ as function of \bar{V}_S for As_2Se_3 EBIC target	34
18 - Plot of $(1-\bar{\delta})$ as function of \bar{V}_S for vidicon tube, $V_T=16$ volts.	35
19 - I_T versus V_T for $I_B = 10^{-6}$ amp. and different input currents	37
20 - I_T versus V_T for $I_B = 10^{-7}$ amp. and different input currents	39
21 - Target signal vs. input current for different values of I_B and $V_T = 50$ volts	40

LIST OF FIGURES (Cont'd)

Figure	Page
22 - Target signal vs. input current for different values of I_B and $V_T = 50$ volts	41
23 - Photographs of display from E-II Ebicon	55
24 - Resolution vs. input illumination for magnetically focused Ebicons	56
25 - Magnetically focused EBIC camera tube with vidicon scan	58

LIST OF TABLES

<u>Table</u>	<u>Page</u>
I) I_T and \bar{V} Values as Function of Target Resistance for a Beam Current of 3×10^{-7} Amperes, $V_T = 40$ Volts.	11
II) EBIC Characteristics of Some Stoichiometric Formulations of As, Se, and S	44
III) EBIC Characteristics of Some Non-Stoichiometric Formulations of As, Se, and S	46
IV) EBIC Characteristics of Some Special Formulations of As, Se, S, and O	47
V) EBIC Characteristics of $CdAs_2Se_4$	48
VI) EBIC Characteristics of Ternary Materials Incorporating Selenium. .	50
VII) EBIC Characteristics of Sb_2S_3 Type Materials.	51
VIII) Summary Of Construction Details of EBICON Tubes	53

1) Introduction

This report summarizes work performed over the past year in the study of thin high gain films of the electron-bombardment-induced conductivity (EBIC) type. The principal emphasis in this work has been on a search for improved EBIC materials, and on a study directed toward obtaining a better understanding of target parameters affecting the quality of scan.

The general objective of the target investigation has been the development of materials having higher gains than were available heretofore, having short decay times as well as the ability to withstand the type of environment associated with camera tube exhaust. High target gain (Ref. 1) is important because it leads directly to improvement in threshold sensitivity for camera tubes using both vidicon and return beam multiplier scan.

The improvement in the ability of a given target to withstand exhaust environment refers to its capability for withstanding exhaust temperatures as well as exposure to cesium and other metallic vapors, associated with the sensitization of photosurfaces. Inability of available target materials to withstand temperatures in excess of 150°C has made it necessary to cool the target during tube bake-out. As a result parts of the tube in the immediate vicinity of the target were not outgassed as well as more remote regions of the tube. In addition there was a tendency for cesium vapors released during sensitization to condense on the cooler parts of the tube. The condensation problem is expected to be a serious one for tubes employing multialkali photosurfaces.

A technique for injecting the target into the tube after the sensitization of the tube has been completed, which is discussed in more detail in the next section, has promise of circumventing the problems associated with the exhaust environment of the tubes. This technique, once perfected, may eliminate the necessity for development of a target which is resistant to the environment present within the interior of a given tube during exhaust.

As noted in a later section, the mechanism for excitation and amplification of photoconductivity (PC) and EBIC type camera tube targets under certain conditions may be somewhat different from that usually stipulated. The mechanism for imaging for vidicon PC type tubes is usually considered to be the following:

The scan surface of the target, in the absence of excitation, is brought by action of the scan beam to a minimum equilibrium potential, $(V_0)_D$ which is near to cathode potential. The target surface after being scanned may be considered to be essentially biased off from the gun, and negligible beam landing occurs. Because of the potential gradient across the target resulting from application of target potential V_T , "dark" current leaks through the target to the backplate. As a result, the potential of the scan surface of the target rises slightly by an amount $(\Delta V)_D$. Hopefully this increase in potential is uniform over the target raster area and information on target non-uniformities is not conveyed to the monitor as a background spurious signal when the scan beam restores the target to its minimum potential $(V_0)_D$.

Manuscript released by authors October 1961 for publication as an ASD Technical Report.

Excitation, whether optical or by high velocity electrons, now increases the number of charge carriers within the target volume, thereby decreasing the resistance of excited areas in proportion to the degree of excitation. As a result the scan surface leaks to a more positive signal potential $(\Delta V)_s$ relative to neighboring dark areas, which as indicated previously reach a maximum potential $(\Delta V)_D$ above the minimum equilibrium potential of the target, $(V_0)_D$. The action of the scan beam now brings all areas of the target back to the equilibrium potential $(V_0)_D$, the effective signal, I_T , from the excited areas being:

$$I_T = \frac{\Delta Q}{\Delta t} = \frac{c \left[(\Delta V)_s - (\Delta V)_D \right]}{\Delta t} \quad (1)$$

where Δt is the time a given raster element having an integrated signal charge ΔQ is scanned, and c is its capacitance. Beam landing occurs only until signal areas are brought to their minimum potential, at which time the target cuts off. The landing current required to charge the target scan surface to $(V_0)_D$ constitutes the video signal. The video signal thus is derived directly from the ability of the beam to land in proportion to the signal voltage strength of a given area. The signal thus generated is capacitively coupled to the backplate where it is fed directly to the preamplifier stage. The mechanism for imaging above described will be referred to henceforth in this report as "signal discharge imaging", since the implication of complete or almost complete signal discharge is present in this imaging mechanism.

During the course of the study of target scan parameters it became evident that signal discharge imaging as described above does not necessarily fully depict the sequence of events responsible for producing video signals for all target materials under all conditions of operation. At least two other effects appear to be involved in the mechanism for producing video signals. All three of the modes of operation are probably usually involved in varying degrees, depending on the condition of the target and the target materials.

The first of the two alternative modes for scan type imaging with PC and EBIC surfaces, which will be described in detail in a later section, will be referred to as target voltage modulation imaging, the other as charge carrier beam modulation imaging. Information on the former mode for imaging derives directly from measurements and analyses which indicate that the scan beam does not necessarily bring signal areas to the same minimum potential $(V_0)_s$ that the dark areas reach as the result of the scan operation. Thus the signal areas are not necessarily discharged or nearly discharged as assumed in "signal discharge imaging".

The target surface does not bias off from the beam and landing occurs through the entire scan interval. The difference in signal response between a dark area and a signal area relates to the average electron absorptivity of the target surface to scan beam electrons as it undergoes a potential shift during the interval beam landing occurs. If the secondary emission ratio which applies to the surface of a given signal area on the target at an

average potential \bar{V}_s is $\bar{\delta}$, then the electron absorptivity of this area of the target to scanning beam electrons may be defined as $(1-\bar{\delta})$, where $\bar{\delta}$ is a function of \bar{V}_s . If I_B is the scan beam current impinging on the target, then the signal current I_T is determined by the magnitude of $I_B(1-\bar{\delta})$. Using this terminology, the magnitude of the dark current will be given by $I_B(1-\bar{\delta})_D$, where $(1-\bar{\delta})_D$ is the electron absorptivity which applies to the average potential of the surface in dark areas of the target. The slope of the $\bar{\delta}$ versus \bar{V} curve turns out to be a significant factor in determining contrast and shades of grey when this type of imaging takes place. When target voltage beam modulation occurs, an increase in I_B or a decrease in $\bar{\delta}$ or both may decrease V_O , the potential of a signal area after scan, until it is substantially equal in magnitude to $(V_O)_D$, the dark current minimum equilibrium potential. Signal discharge imaging will then occur, since the condition for full discharge of a signal area is then met. It is evident that the signal discharge mode of imaging is a special case of the target voltage modulation mode.

The term charge carrier beam modulation imaging derives directly from measurements described in a later section which indicate that the electron absorptivity of the target for slow electrons may be significantly affected by the excitation conditions which occur in a given area of the target. It is likely that the number of excited charge carriers and the distribution of trapping and recombination states, affect the retention capabilities of the targets as far as the low velocity electrons of the scan beam are concerned. In this mode of imaging the target absorptivity to scan beam electrons is affected both by the average potential of the target surface and by the conditions of carrier excitation. There is also evidence to indicate that the scan beam electrons which are absorbed or retained by the target can affect the conductivity of certain targets. It is evident that further study of the various mechanisms associated with charge carrier scan beam modulation is required.

It is believed that the work on scan variables, described in a later section, will benefit the program from the standpoint of assisting in the understanding of target parameters which are beneficial for imaging, as well as in the determination of whether parameters useful for vidicon scan are the optimum parameters for scan using a return beam multiplier. In addition this work should materially contribute to the development of techniques for evaluating the performance of a given target, which is a prime necessity to the target research program.

2) Army Signal Corps Program

The work performed for the Signal Corps on Contract DA-36-039 SC-87397 during the past period has been largely concerned with the study of factors affecting the performance of an EBIC camera tube having a multiplier in the return beam. This work has encompassed (a) A study of factors limiting the resolution of the scan section, (b) A study of scan parameters as they affect EBIC target performance. The aspects of this work which are pertinent to the evaluation of targets has a common basis with the Air Force Program and is

summarized in Section 3 of this report. (c) Work on magnetically focused high voltage image sections. (d) A detailed study of the properties of As_2S_3 and As_2Se_3 type EBIC targets. (e) The work referred to previously on developing a method for injecting the EBIC target into the EBIC camera tube. This technique involves storing the target in a protected location in a side tubulation until the tube is outgassed, the photosurface is sensitized, and the tube is ready to be tipped off the pumps. A major problem has concerned the developing of techniques to seal off the connecting tubulation. This technique has been reasonably successful and has been applied to experimental tubes fabricated on the Air Force program which will be described later in this report.

3) Investigation of Scan Parameters as They Affect Target Performance*

a. Simplified Theory of Target Scan

When a camera tube having a photoconductive or an EBIC type target is employed for continuous imaging of a fixed scene, an equilibrium condition is reached in which the amount of charge deposited by the beam is equal to the amount of signal charge which leaks from the scan surface to the backplate of the target.

This equilibrium may be described by the following equation:

$$I_T = \frac{V_T - \bar{V}_s}{R} = I_B(1-\delta) \quad (2)$$

where I_T is the average target signal current, V_T is the target backplate voltage, \bar{V}_s is the average DC potential reached by the target surface. R is the total effective resistance of the excited target in ohms; I_B is the magnitude of the beam current landing on the target, in amperes, and δ is the value of the secondary emission ratio which is applicable to the average surface potential of the target \bar{V}_s . In the following the assumption is made that δ is a function of \bar{V}_s only and not of other parameters such as the input excitation.

An equation similar to (2) applies to the dark current which is drawn through the target in the absence of excitation:

$$(I_T)_D = \frac{V_T - \bar{V}_s}{R_D} = I_B(1-\delta) \quad (3)$$

where $(I_T)_D$ and R_D are the target current and resistance associated with the unexcited target under scan conditions.

* This section summarizes work performed under joint sponsorship of Signal Corps on Contract DA-36-039 SC-87397 and WADD on Contract AF 33(616)-6496.

The contributions to beam velocity produced by the Maxwellian distribution of electrons leaving the hot cathode, and contact potential effects have been neglected in this analysis. The effect of these variables on target performance has been discussed in Ref. (1). This reference also includes a more general treatment of target scan parameters than is presented here.

The electric field gradients across PC and EBIC targets (which are of the order of 50,000 to 500,000 volts/cm) exceed those in the case of common semiconductors such as Ge and Si for which Ohm's law normally applies (1,000-10,000 volts/cm). For materials having low band gaps, when the velocity imparted to the electrons in one mean free path becomes comparable to the thermal velocities of the electrons in the solid, substantial departures from Ohm's law have been observed (Ref. 2,3). The mobility of the charge carriers in these materials exhibits an $E^{1/2}$ power relationship after a critical gradient is exceeded. In order for Ohm's law to hold, the number of charge carriers and the mobility of these carriers should be independent of the field gradient. Apparently the conditions for Ohm's law to apply are approximately filled at high field gradients in certain photoconductors which have relatively large values of band gaps. Amorphous selenium has been observed to meet the conditions for ohmic behavior when exposed to low intensity illumination (Ref. 4). At higher excitation levels, the target current varies according to the square of the voltage across the target, a relationship consistent with the passage of space-charge-limited currents.

The photo-excited currents in Sb_2S_3 photoconductive materials have been found to vary with the first power of voltage across the target (Ref. 5), which is indicative of ohmic behavior. At fixed values of EBIC excitation, the variation of signal currents through As_2S_3 targets (Ref. 1) with the voltage impressed across the target can also be approximated by a first power relationship. Similarly, many of the other experimental materials investigated show the same approximate relationship. Ioffe (Ref. 6) has observed that the photoconductive conductivity is independent of the field gradient for pure materials. However, the experimental work apparently did not exceed gradients of 45,000 volts/cm.

In view of the above, the assumption is made in the following analysis that the behavior of PC and EBIC materials under excitation follow Ohm's law. In the case of non-ohmic behavior it is necessary to perform an averaging operation on eqs. (2) and (3) in which the variation of the target resistance with field is considered.

As a result of the leakage type signal currents, which are characteristic of PC or EBIC type targets, the instantaneous value of target surface potential under uniform continuous excitation will rise from a minimum value V_0 to a maximum value of surface potential V_m during frame time. Under equilibrium conditions the deposition of electrons from the

gun during the scan interval will reduce the surface potential back to V_0 immediately upon conclusion of the scan action on any given target element. This equilibrium condition may be represented mathematically by the following equation:

$$(\Delta Q)_W = (\Delta Q)_R = \Delta VC = (V_m - V_0)C = I_T T \quad (4)$$

where $(\Delta Q)_W$ and $(\Delta Q)_R$ represent the electrical charge transported during the writing and reading operations, $\Delta V = (V_m - V_0)$ is the change in potential produced as a result of the writing and reading actions, T is frame time, and C is the capacity of the target raster.

Using standard condenser discharge equations, the instantaneous potential of the target surface during the writing interval may be expressed by the following equation:

$$V_s = V_T - (V_T - V_0)e^{-t/RC} \quad (5)$$

where $V_s = V_0$ at $t = 0$. Since the target surface reaches V_m potential at the completion of the writing interval T ,

$$V_m = V_T - (V_T - V_0)e^{-T/RC} \quad (6)$$

and

$$\Delta V = V_m - V_0 = (V_T - V_0)(1 - e^{-T/RC}) \quad (7)$$

$$V_0 = V_T - \frac{\Delta V}{(1 - e^{-T/RC})} \quad (8)$$

As beam current I_B is increased, V_0 will decrease until it approaches a minimum equilibrium value which is very close in magnitude to $(V_0)_D$, the potential of dark areas of the target immediately after being scanned. $(V_0)_D$ and hence V_0 for high I_B is assumed to coincide with the zero reference of potential for target backplate voltage. Thus for the condition of high beam eq. (8) becomes:

$$V_T = \frac{\Delta V}{(1 - e^{-T/RC})} \quad (9)$$

Expressing eq. (9) in terms of R, and expanding in a series,

$$R = -\frac{T}{C} \frac{1}{\ln(1 - \frac{\Delta V}{V_T})} = \frac{T}{C \left(\frac{\Delta V}{V_T} + \frac{1}{2} \left(\frac{\Delta V}{V_T} \right)^2 + \dots \right)} \quad (10)$$

Neglecting the higher power terms, and substituting for V using eq. (4), we obtain for the case of high beam:

$$R = \frac{TV_T}{C\Delta V} = \frac{V_T}{I_T}, \quad (11)$$

which is also the expression obtained by use of eq. (2) assuming V_s is zero due to high beam.

In order to determine the corresponding equations for action of the scanning beam, it is necessary to have a knowledge of the variation of the secondary emission ratio as a function of V_s . The typical variation of secondary emission ratio with surface potential^s can be approximated by an equation of the following form:

$$\delta = 1 - aV_s + bV_s^2 \quad (12)$$

Consider a raster element having capacity C_R . If it is exposed to the beam for time t, the element will decrease in potential from V_m to V_s according to the equation:

$$C_R (V_m - V_s) = \int_0^t I_B (1 - \delta) dt. \quad (13)$$

Differentiating:

$$-C_R \frac{dV_s}{dt} = I_B(1 - \delta) = I_B(aV_s - bV_s^2). \quad (14)$$

By integrating for the time τ_o required to scan a raster element, the following equation is obtained:

$$\left(\frac{a-bV_o}{V_o}\right) = \left(\frac{a-bV_m}{V_m}\right) e^{\frac{aI_B \tau_o}{C_R}}. \quad (15)$$

Since the ratio $\frac{\tau_o}{C_R}$ can be approximated by $\frac{T}{C}$, eq. (15) may be expressed as follows:

$$\left(\frac{a-bV_o}{V_o}\right) = \left(\frac{a-bV_m}{V_m}\right) e^{\frac{aI_B T}{C}} \quad (16)$$

For the low voltage portions of the δ vs V_s curves, the last term in eq. (12) can be neglected, and eq. (16) takes the form:

$$V_o = V_m e^{\frac{-aI_B T}{C}} \quad (17)$$

By using the equality

$$\Delta V = (V_m - V_o) = \frac{I_B T}{C}, \quad (18)$$

eq. (16) can be solved for V_o giving:

$$V_o = \frac{a}{2b} - \frac{\Delta V}{2} \pm \frac{1}{2} \sqrt{\left(\frac{a}{b}\right)^2 - 2\left(\frac{a}{b}\right) \Delta V + (\Delta V)^2 - \frac{4I_B T}{bI_B}}. \quad (19)$$

In solving eq. (16) for V_o , the exponential is expanded into a power series, Little loss in accuracy is obtained when the first two terms of the series are used for values of (aI_T/C) less than 0.1, which are usually the case.

The average surface potential \bar{V}_s can be obtained directly from eqs. (2) and (12) as follows:

$$I_T = I_B (1 - \delta) = I_B (a\bar{V}_s - b\bar{V}_s^2). \quad (20)$$

Solving the above quadratic for \bar{V}_s gives

$$\bar{V}_s = \frac{a}{2b} \pm \frac{1}{2} \sqrt{\left(\frac{a}{b}\right)^2 - \frac{4}{b} \frac{I_T}{I_B}} \quad (21)$$

Substituting in eq. (12) for $\delta = 1$, it is evident that the first crossover potential corresponds to a/b volts. By differentiating this equation, it is evident that the minimum potential on the curve of δ vs. \bar{V}_s which will be defined as $(V_s)_o$, is equal to $a/2b$ volts.

Equations (8) and (19), which are derived from the scan and writing parameters respectively, together with eq. (18), define the general performance of a scan system under equilibrium between the scan and writing actions.

While \bar{V}_s can be determined as a function of I_T from simple scan parameters, in order to determine V_o it is necessary also to have a knowledge of factors affecting wave form, such as frame time T and the capacitance of the target. Since ΔV in most EBIC applications is substantially under a volt, a fairly close approximation to the potential situation on the target can be obtained by assuming $V_o = \bar{V}_s - \Delta V/2$, and $V_m = \bar{V}_s + \Delta V/2$.

A better understanding of the target parameters can be obtained by utilizing a specific functional relationship between δ and \bar{V}_s . The typical δ function shown at the left of Fig. 1 is based on the following equation:

$$\delta = 1 - 1.7 \times 10^{-2} \bar{V}_s + 2.8 \times 10^{-4} \bar{V}_s^2 \quad (22)$$

The variation of I_T and \bar{V}_s as a function of V_T shown in Fig. 1 has been determined using eq. 2, assuming that eq. (22) applies to the surface, and that the target resistance is 10^9 ohms. It is evident that the resistance of the target is only one of the variables which determines the signal current for a given value of backplate voltage. The maxima on the signal

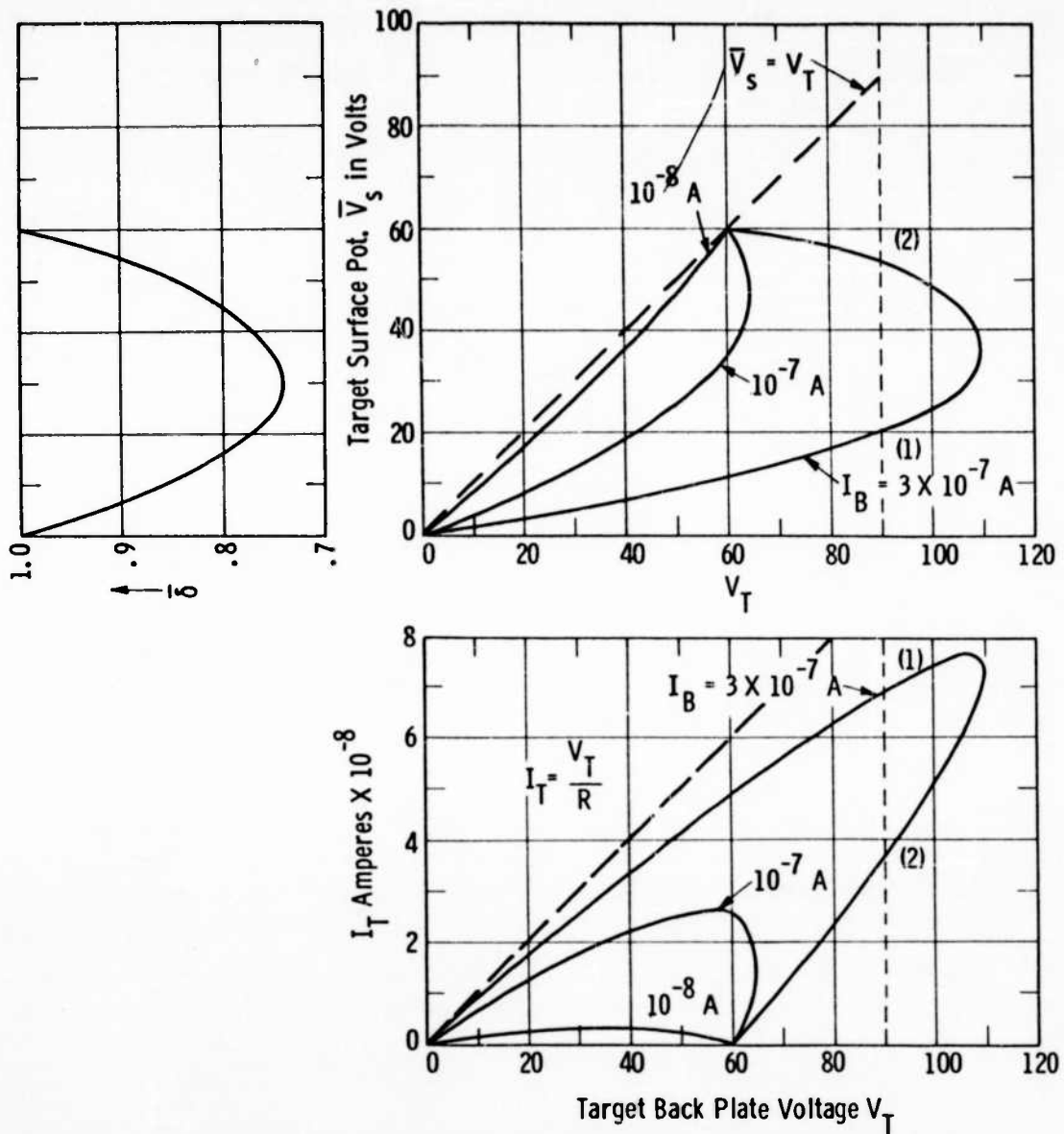


Fig. 1--EBIC target scan parameters assuming target resistance $R = 10^9$ ohms and $\bar{\delta} = 1 - 1.7 \times 10^{-2} \bar{V}_s + 2.8 \times 10^{-4} \bar{V}_s^2$; for indicated values of I_B .

versus target backplate potential curves always correspond to the value of target surface potential, $(\bar{V}_s)_0$, for which the potential difference across the target, $(V_T - V_s)$, is a maximum. The maximum possible signal current is thus given by the product of I_B by the $(1-\delta)$ value which corresponds to $(V_s)_0$. It is interesting to note that the maximum signal is not determined by the target resistance or backplate potential.

The curves of Fig. 2 have been derived for a fixed beam current of 3×10^{-7} amperes. Different values of target resistance between 10^8 and 2×10^9 are assumed. The constancy of the maximum value of (I_T) observed in this figure despite the variation of R graphically illustrates that the specific value of the maximum is dependent only on $I_B (1-\delta)$ max. Referring to the upper curve of Fig. 2, it is evident that the I_T maxima all occur at $\bar{V}_s = 30$ volts, as would be expected.

The I_T vs V_T curves of Fig. 1 will be observed to approach a limiting curve defined by eq. (11) as I_B is increased. Signal discharge imaging as defined previously would be expected to take place as I_T approaches the limiting curve, and \bar{V}_s approaches zero potential.

From Fig. 2 for a beam current of 3×10^{-7} amperes and a target backplate voltage of 40 volts, it is evident that signal currents in excess of 10^{-8} amperes involve appreciable values of \bar{V}_s . Table I below lists the I_T and \bar{V}_s values associated with the different values of target resistance shown in Fig. 2. The column at the right-hand side of this table gives ΔV on the assumption that the raster is that of a standard vidicon having an area of $3/8" \times 1/2"$. A 2μ target thickness is assumed and a dielectric constant of 6.25.

TABLE I

I_T and \bar{V}_s Values as Function of Target Resistance for a Beam Current of 3×10^{-7} Amperes, $V_T = 40$ volts.

R(ohms)	I_T (amperes)	\bar{V}_s (volts)	ΔV (volts)
2×10^9	1.8×10^{-8}	3.0	.18
10^9	3.3×10^{-8}	7	.33
6×10^8	4.8×10^{-8}	11	.48
3×10^8	6.6×10^{-8}	20	.66
10^8	7.7×10^{-8}	32	.77

From this table it is evident that a target having secondary emission characteristics defined by eq. (22) will require beam currents substantially in excess of 3×10^{-7} amperes if signal discharge imaging is to be

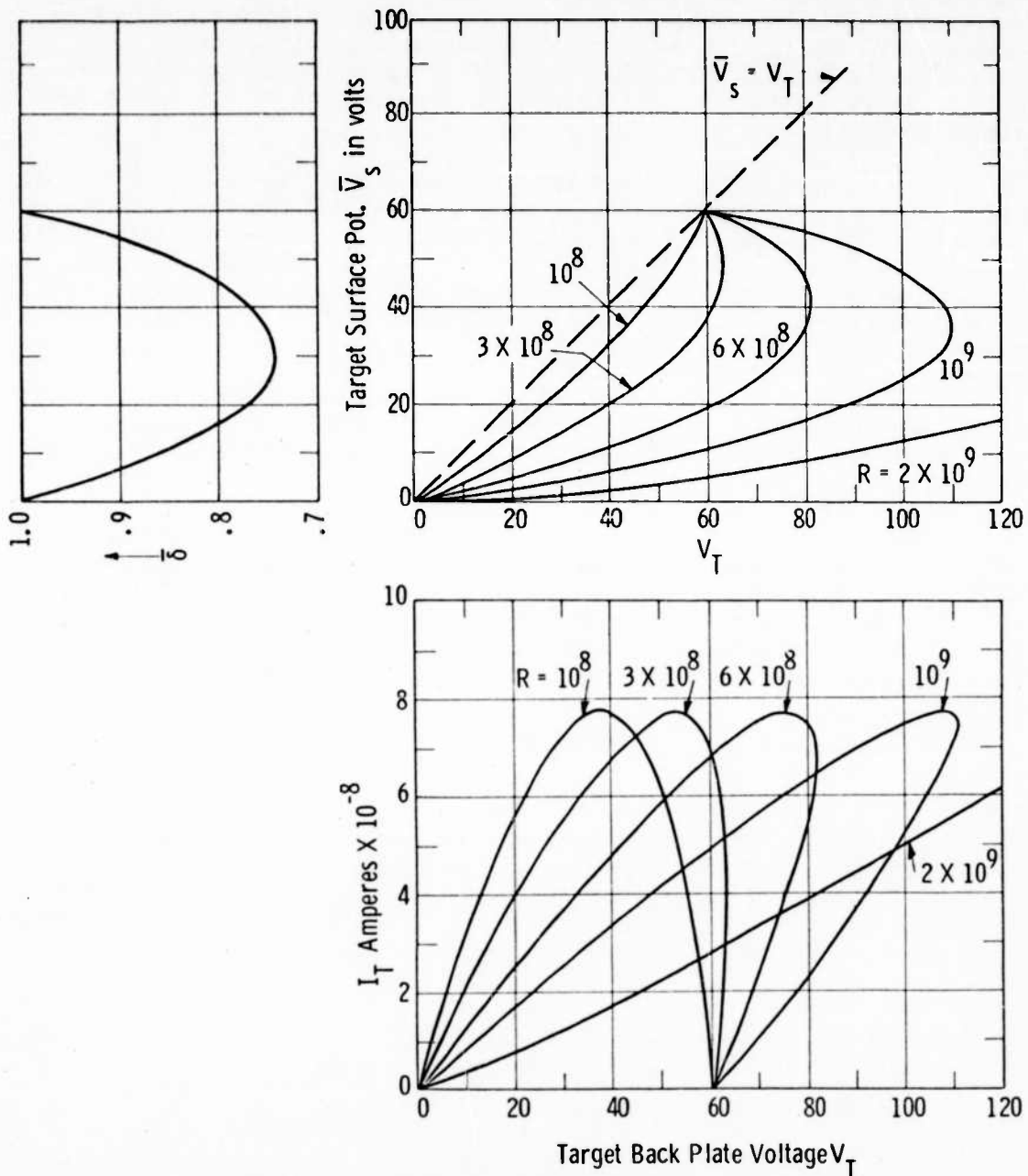


Fig. 2--EBIC target scan parameters for $\bar{\delta} = 1 - 1.7 \times 10^{-2} \bar{V}_s + 2.8 \times 10^{-4} \bar{V}_s^2$, the indicated values of target resistance in ohms and $I_B = 3 \times 10^{-7}$ A

approached. For the 3×10^{-7} amperes beam current used in Table I, target voltage modulation imaging, as defined previously, will occur. In this mode of imaging the secondary emission characteristic of the surface play an important role in determining the signal and contrast levels attained. In signal discharge imaging on the other hand, the secondary emission characteristics of the target determine the amount of beam required to attain this form of imaging, but play no further role in determining the imaging characteristics of the target.

It is interesting to note that the ratio of the highest to the lowest resistance in Table I is 5, and that the corresponding ratio for signal current is only 4.53. This is equivalent to .94 power variation of signal current with input excitation. The departure from first power variation is related only to the secondary emission characteristic of the target surface, and does not involve solid state parameters.

A graph of the type shown in Fig. 3 is useful for visualizing the effect of the various parameters involved in the scanning of PC and EBIC type targets. The beam landing and remaining on target, $I_B(1-\bar{\delta})$, is plotted for various beam currents as a function of \bar{V}_S , where $\bar{\delta}$ is assumed to be defined by eq. (22). The target leakage current, obtained from the equation $(V_T - \bar{V}_S)/R$, is also plotted on the same graph as a function of \bar{V}_S . The load lines shown in the diagram correspond to all the possible average leakage currents through the target for target resistances of 2×10^9 and 10^{10} ohms and a backplate potential of 50 volts. These load lines are fixed by the knowledge that the signal current is zero when $\bar{V}_S = V_T$, and equal to V_T/R when $\bar{V}_S = 0$.

The intersection of a given load line with an $I_B(1-\bar{\delta})$ curve represents a possible point of equilibrium, since the leakage current through the target is equal to the current deposited by the beam at this point in the diagram. When the target backplate potential is greater than the first crossover potential of the target, a given load line will make two intersections with a given beam landing line, one above $(\bar{V}_S)_0$, the other below it. Intersections or operating points which occur below $(\bar{V}_S)_0$ meet the criteria for stable equilibrium situations since any departure of \bar{V}_S from the values corresponding to the intersection points will produce a flow of charge which will restore \bar{V}_S to its equilibrium value. For example, if \bar{V}_S fluctuates for any reason below the equilibrium value corresponding to a given operating point, it is evident from Fig. 3 that the target leakage current will increase, and the beam landing current will decrease. Both of these changes are in a direction which makes the target more positive and restore the signal potential. Similarly for any fluctuation of surface potential which makes \bar{V}_S more positive than the potential corresponding to the intersection of the two curves, the landing current increases and the target leakage decreases, both effects again working toward shifting surface potentials back to equilibrium values.

Quite a different situation occurs for operating points above $(\bar{V}_S)_0$. A fluctuation in \bar{V}_S which is more negative than the expected operating potential, will increase both the beam landing and the target leakage currents. From Fig. 3 it is evident that the beam landing will increase more rapidly than the target

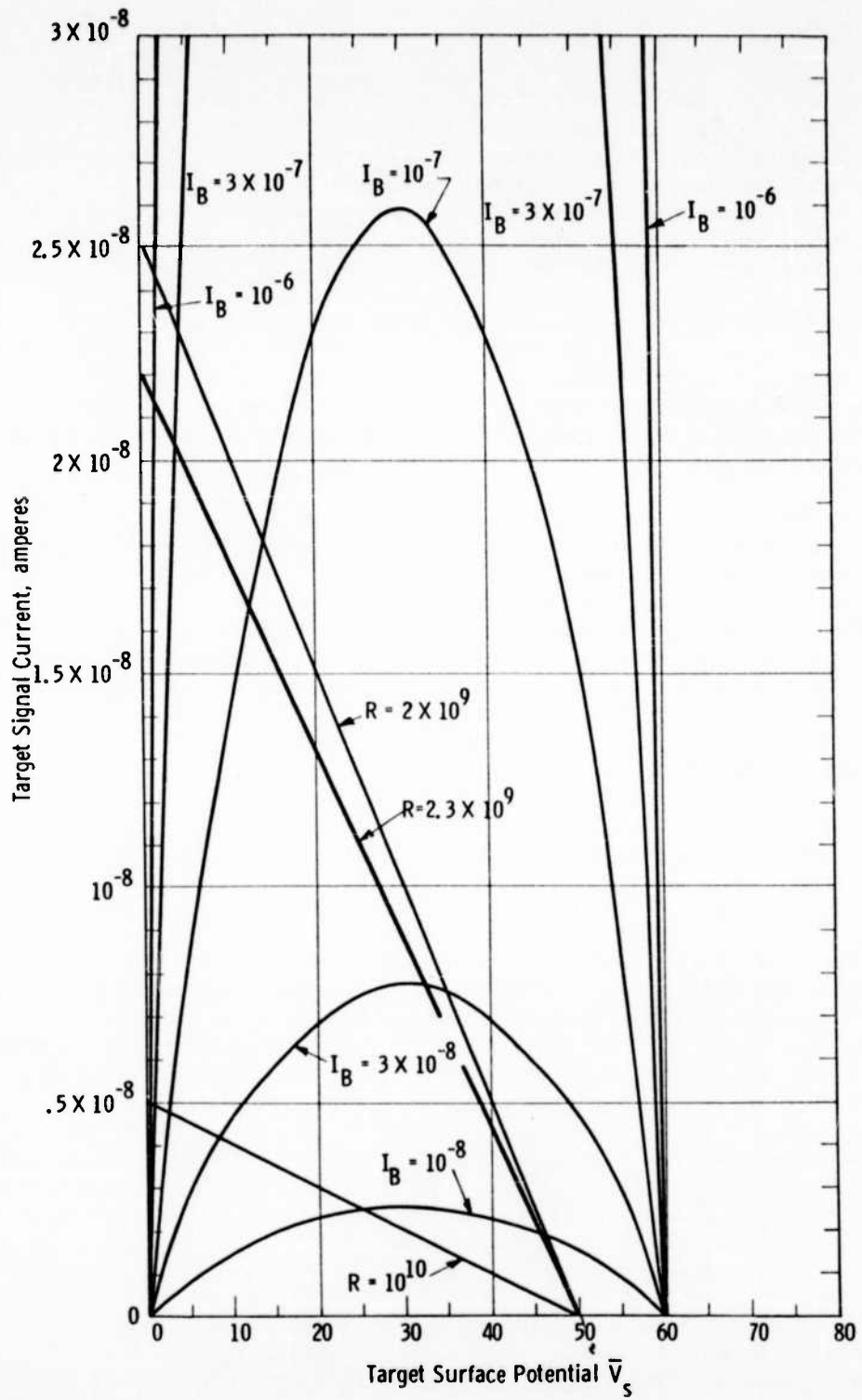


Fig. 3--As function of \bar{V}_s : Target leakage currents for different values of target resistance; also beam landing signal $I_B (1-\delta)$ for different values of I_B .

leakage currents. Thus the target surface potential would shift progressively further away from the intersection value of \bar{V}_S toward the stable operating point below $(\bar{V}_S)_0$. Similarly, for fluctuations of \bar{V}_S above the intersection value, the beam landing current will decrease more rapidly than the target leakage current, and the target surface would be expected to shift in the more positive direction away from the intersection potential and toward the first crossover point. Thus intersections of the curves of Fig. 3 which occur below $(\bar{V}_S)_0$ may be expected to correspond to stable operating points, and those above $(\bar{V}_S)_0$ to unstable operating points.

Referring to Fig. 1, for $V_T = 90$ volts, the points on the curves marked (1) correspond to stable and those marked (2) to unstable operating points.

The changes in I_T and \bar{V}_S respectively as a function of I_B for a target backplate potential of 50 volts and different values of target resistance are shown in Figs. 4 and 5, again assuming that the secondary emission ratio of the surface is defined by eq. (22). The signal current curves saturate at high values of I_B as would be expected from Fig. 3. The plateau portions of the I_T vs I_B curves correspond to low values of \bar{V}_S . Any significant drop in I_T as I_B is decreased is, however, an indication of a substantial rate of rise in the value of \bar{V}_S .

Considerable information on a given target material can be obtained by making measurements corresponding to the plots of Fig. 4. The electron absorptivity of the target surface, $(1-\delta)$, for any given operating point is obtainable directly from the ratio I_T/I_B . To obtain the corresponding values of \bar{V}_S , it is necessary only to solve eq. (11) for R using the saturated values of I_T , and to substitute the value so obtained in the equation $\bar{V}_S = V_T - I_T R$ to obtain \bar{V}_S .

When the positive excursion of \bar{V}_S is restricted by use of sufficient high values of I_B , the low voltage portion of the δ vs \bar{V}_S curve can be approximated by an equation of the form:

$$\bar{\delta} = 1 - a\bar{V}_S \quad (23)$$

Using eq. (2) and eq. (23) the following expressions for \bar{V}_S and I_T can be obtained:

$$\bar{V}_S = \frac{V_T}{(1 + aI_B R)} = \frac{I_T}{aI_B} \quad (24)$$

$$I_T = \frac{V_T}{R} \frac{(aI_B R)}{(1 + aI_B R)} \quad (25)$$

When $aI_B R$ is large, as in the case of high beam, or high target resistance, or high value of "a", eq. (25) transforms into eq. (11). If we arbitrarily define signal discharge imaging as occurring when \bar{V}_S is less than 1 volt, then

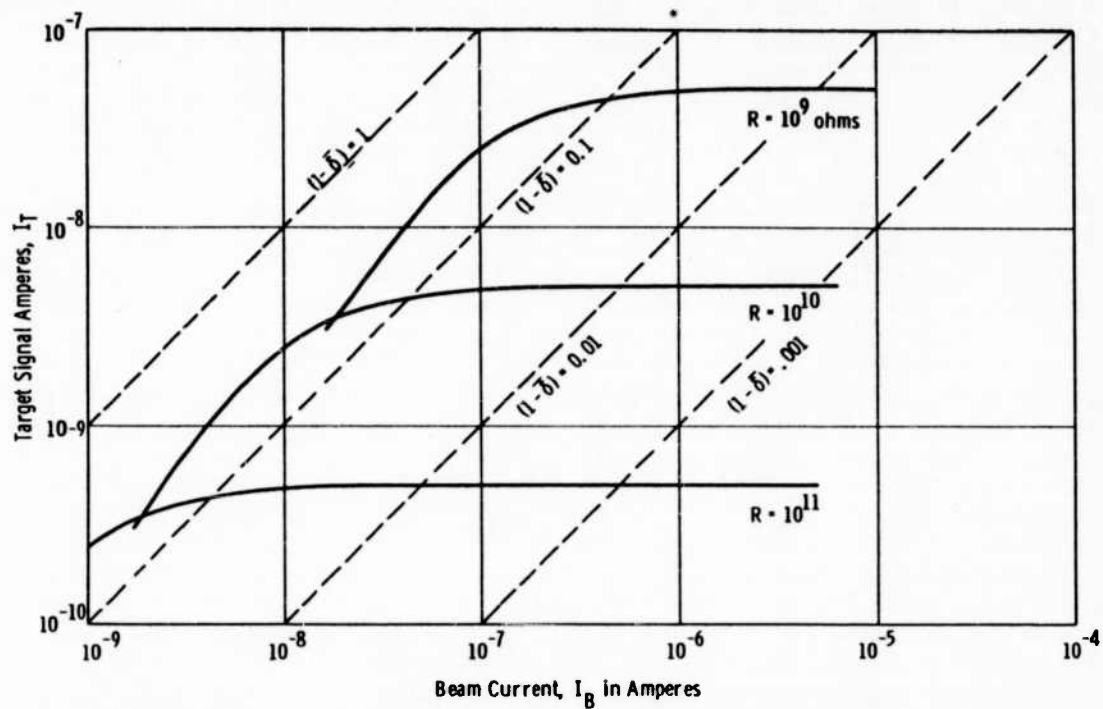


Fig. 4— Target signal current as function of beam current for various values of target resistance.
 Assumes $V_T = 50$ volts and $\bar{\delta} = 1 - 1.7 \times 10^{-2} \bar{V}_s + 2.8 \times 10^{-4} \bar{V}_s^2$.

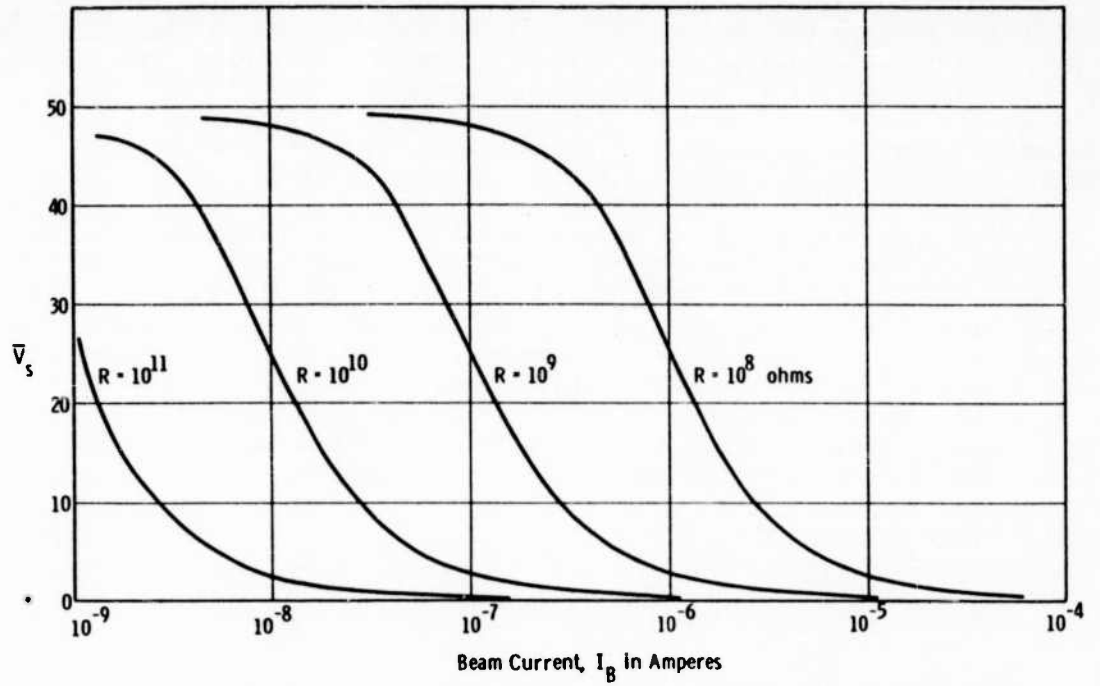


Fig. 5--Target surface potentials as function of beam current for parameters of Fig. 7.

from eq. (24) this condition is met when:

$$aI_B R \geq (V_T - 1) \quad (26)$$

The visual effect of varying \bar{V}_S by changing I_B at a given constant excitation can be observed on the monitor of the camera tube. As I_B is reduced from a relatively high value, little effect is observed initially corresponding to the saturation region, where little change in I_T occurs as I_B is initially decreased. A critical beam current is then reached below which the whites in the image are observed to diminish in brightness. Contrast then goes down markedly.

With some target materials it is possible to observe a definite gradation in the white areas at low values of I_B , which it is believed is attributable to beam bending. The image consists of black and white areas of reduced contrast due to the low beam. However, the white areas adjacent to the blacks are whiter than white areas which are more remote from the blacks. It is believed that the darker parts of the white areas have \bar{V}_S values which are greater than $(\bar{V}_S)_0$. The whiter areas in the white images have had greater beam landing due to bending the beam directed at the blacks. Thus these areas have a lower \bar{V}_S value than the white areas which are remote from the blacks, and thus have greater values of $(1-\bar{\delta})$ and in consequence greater signal. Further diminishing of beam will cause the whiter areas of the white to blend into the blacks, and full image reversal is now experienced. The failure of the beam to land on the black areas due to beam bending has contributed substantially in the building up of the \bar{V}_S value of the black regions of the image.

The rate of increase of \bar{V}_S and decrease in I_T with decreasing I_B can also be assessed using Fig. 3. It is evident as I_B is decreased not only does I_T decrease but signal contrast, as given by $[(I_T)_2 - (I_T)_1]/(I_T)_2$, also decreases, where $(I_T)_2$ and $(I_T)_1$ represent the signals associated with load lines corresponding to R_2 and R_1 ohms target resistance respectively. Depending on the resistance of the load lines selected, image contrast not only reduces with decreasing I_B but also can reverse in polarity, i.e., a grey area at low I_B values can furnish a higher signal output than the signal highlight area. If reversal occurs at very low I_B values, it is also evident that as I_B is reduced a range of signal levels will occur wherein the white area is equal to and hence indistinguishable from the image corresponding to the grey area.

By inspection of Fig. 3 it is apparent that it is desirable in the interest of large signals to operate at the highest possible target backplate voltage. Ordinarily, V_T is limited by target non-uniformities, and by the possibility of parts of the target going over first crossover potential. It is also evident that it is desirable to utilize the highest beam possible. However, in the case of a tube with a return beam multiplier, as noted in Ref. (1), beam noise increases as $I_B^{1/2}$. Also, the scanning beam spot size tends to increase as beam level is increased. For these reasons, depending on the parameters of the target and the

input signal level used, an optimum value for setting of beam current will exist. In tube operation this is normally determined by adjusting beam current to produce optimum image quality at a given signal input level from the scene.

b. Experimental Investigation of Target Scan Parameters

In the previous section, a simplified theory of operation of EBIC and PC type targets was developed. In the derivation the secondary emission ratio of the target surface was assumed to be a function only of \bar{V}_S and not, for example, of the target excitation level. Characteristic curves were plotted assuming a specific relationship between $\bar{\delta}$ and \bar{V}_S which was considered to be typical of an insulating material. It is evident that the general mechanism for imaging developed should in general be independent of the particular functional variation of $\bar{\delta}$ with respect to \bar{V}_S .

The simple theory assumed that the targets exhibit ohmic behavior, and that target resistance is a function only of the input excitation and not dependent, for example, on the voltage impressed across it, nor the magnitude of the beam current going to it. The accuracy of the determination of \bar{V}_S depends on the extent these assumptions hold. As indicated later in this section, it is believed that the assumption of ohmic response is a reasonable approximation for the field gradients which occur across the target on the measurements described here.

The method outlined in the previous section for determining target resistance and electron absorptivity of the target surface is employed in the present section to determine scan parameters of specific target materials, and to check the validity of the assumptions previously made.

The accuracy of the determination of $(1-\bar{\delta}) = I_T/I_B$ in these measurements is largely a function of how accurately I_B can be determined and the amount of drift experienced during a given set of readings. After comparative tests of different methods of determining I_B , the method finally used involved the measurement of the current to the focus electrode of the vidicon scan gun with the magnetic focus field off, and then making allowances for the anticipated electron transmission of the mesh structure at the extremity of the focus electrode.

An attempt was initially made to take $(1-\bar{\delta})$ characteristics of As_2S_2 and As_2S_3 targets using target dark current as the "signal" current. The attempt was abandoned when it was found that the dark current was so low for these materials it could not be determined in the demountable position in which the measurements were made. The $(1-\bar{\delta})$ determinations were then made of these materials under constant EBIC excitation. The need for constant excitation increased the difficulty of making accurate measurements, since the input current tended to drift and the measuring circuit had a relatively long time constant.

When EBIC excitation is used to obtain measurable target signal currents, it is necessary to correct the magnitude of the beam current so that it corresponds

to the beam current going to the excited areas only. For the measurements reported here, the ratio of the total scanned area to the excited area of the target was 4.4. In this report measurements of $(1-\bar{\delta})$ in which the total beam current have been corrected to correspond to the actual beam landing on the excited areas are referred to as "actual" $(1-\bar{\delta})$ measurements; whereas the uncorrected ones are referred to as "video" type measurement, since they are made under typical video conditions. Unless stipulated specifically otherwise, all measurements in this report are of the "video" type. The $(1-\bar{\delta})$ values can be converted to actual readings by multiplying by 4.4. Similarly, when EBIC excitation is used to energize a given target, the "actual" beam current to the excited area can be obtained by dividing the indicated video beam current by 4.4.

Experimental I_T vs I_B curves for an As_2S_2 target (581AR1) are plotted in Fig. 6 for different constant EBIC excitation. The curves are quite similar in shape to the curves calculated in Fig. 4 on the basis of a surface having the $(1-\bar{\delta})$ characteristics defined by eq. 22. As I_B was reduced at higher levels of excitation the image polarity reversed showing that $(V_s)_0$, the minimum on the $\bar{\delta}$ vs \bar{V}_s curve, was being approached. The filled-in points on the curves indicate the presence of reversed polarity images. The apparent \bar{V}_s and $(1-\bar{\delta})$ values corresponding to the first reversed image on the 8×10^{-11} ampere excitation curve can be obtained using eq. (2) as follows:

$$I_T = \frac{V_T - \bar{V}_s}{R} = \frac{50 - \bar{V}_s}{8.3 \times 10^8} = 1.7 \times 10^{-8}$$

$$\bar{V}_s = 35.9 \text{ volts}$$

$$\text{and } \frac{I_T}{I_B} = \frac{1.7 \times 10^{-8}}{9 \times 10^{-8}} = .19$$

The target resistance as a function of the EBIC excitation input current was calculated using eq. (11) for the 4 lower curves of Fig. 6 on the assumption that signal saturation as a function of beam current was obtained on these curves. The resulting values of target resistance under excitation have been plotted as the lower curve in Fig. 7 as a function of input current. Also shown in Fig. 7 are target resistance values for As_2S_3 targets under excitation as a function of input current, which were obtained in similar fashion. The excited area of the target was approximately 0.5 cm^2 in area. Thus the resistivity of the target material can be obtained at a given excitation by multiplying the computed resistance by $10^4/2d$, where d is in microns. Since target 581AR1 was 1.6μ , this factor is equal to 3.1×10^3 . From separate data the dark resistance of the targets lies between 10^{15} to 10^{16} ohm-cms.

On the assumption that target resistance at a fixed value of excitation does not change as a result of the variation in target field gradients with change in beam current, $(1-\bar{\delta}) = I_T/I_B$ has been calculated as a function of \bar{V}_s , where \bar{V}_s is determined from the relationship $\bar{V}_s = V_T - I_T R$. The $(1-\bar{\delta})$ values

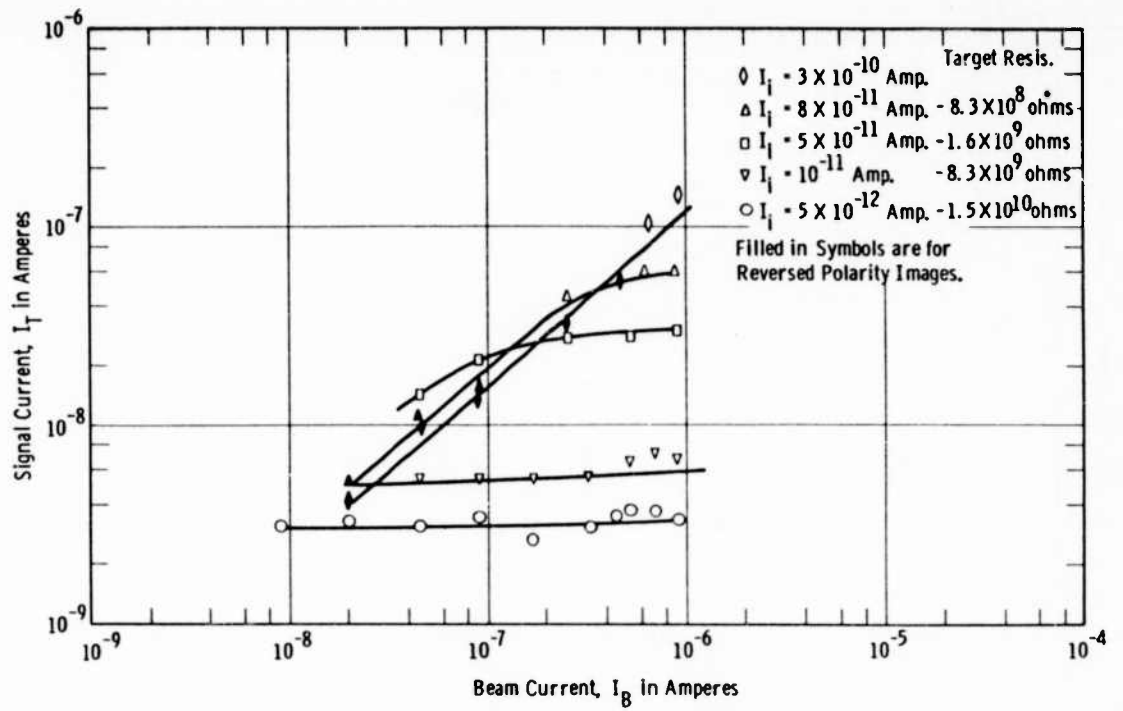


Fig. 6—EBIC signal current for As_2S_3 target as function of input current (target 581 AR1, $V_T = 50$ volts)

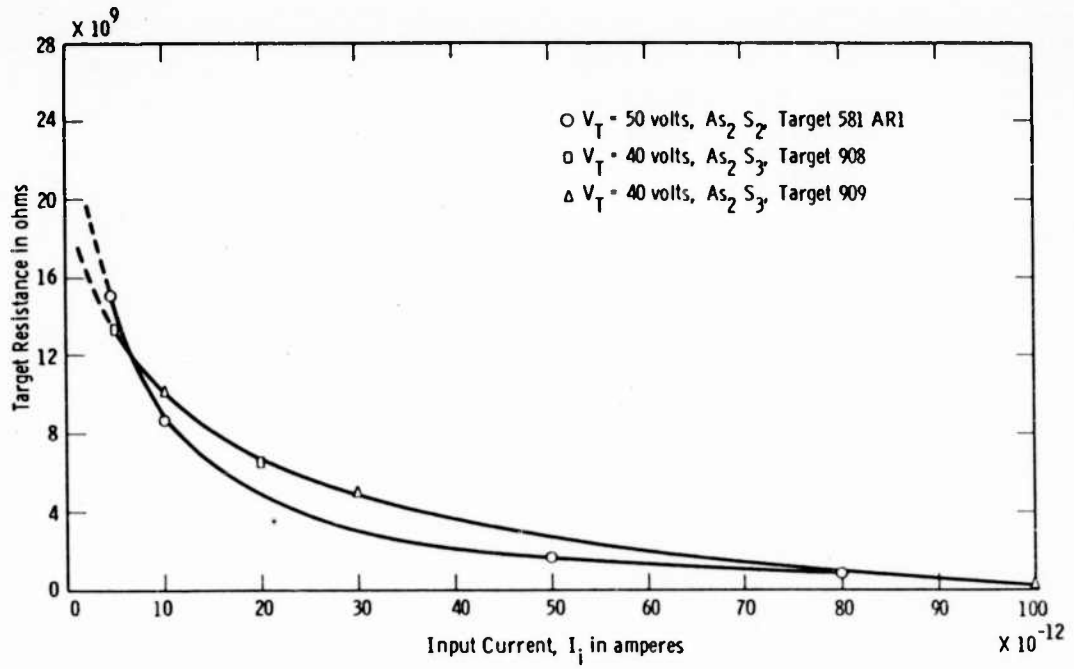


Fig. 7 --Resistance of $As_2 S_3$ and $As_2 S_2$ EBIC targets as function of input current

corresponding to input currents of 8×10^{-11} , 5×10^{-11} , and 10^{-11} amperes are plotted as a function of \bar{V}_s in Fig. 8. Reasonable agreement between the different curves may be observed in the region of low \bar{V}_s . The upper curve can be approximated between the origin and 20 volts by a straight line having the equation $1-\bar{\delta} = 1.25 \times 10^{-2} \bar{V}_s$.

The knowledge of \bar{V}_s for various values of I_B and I_1 is used in plotting Fig. 9. In this figure, \bar{V}_s is plotted as a function of I_1 for I_B values of 10^{-6} , 10^{-7} and 10^{-8} amperes respectively, assuming $a = 1.25 \times 10^{-2}$ volts $^{-1}$. It is pertinent to point out that once the constant a has been evaluated, \bar{V}_s can be obtained very simply from a knowledge of I_T using eq. (24), recognizing that this equation holds only in the region where the $(1-\bar{\delta})$ curve versus \bar{V}_s can be approximated by a straight line, i.e., between 0 and 20 volts.

The discrepancies in the $(1-\bar{\delta})$ values at high values of \bar{V}_s input excitation raises the question as to whether the differences in the measurements were due to non-ohmic behavior of the targets, to the influence of charge carriers, filled states, etc., within the forbidden band of the target material as a function of the excitation, or possibly to inaccuracy of measurements due to the factors described previously.

Accordingly, the series of measurements plotted in Fig. 10 for an As_2S_2 target were made at 10^{-10} and 3×10^{-11} ampere input excitations. The readings were repeated several hours later with fairly good agreement being obtained. The measurements shown on the bottom curve of the figure were made at 2×10^{-12} amperes input excitation. This curve indicates that an apparently real substantial diminution in the electron absorptivity of the target occurs at very low excitations. Evidently, the particular As_2S_2 target employed has a high reflectivity for electrons when charge carriers are not present. The presence of charge carriers or some effect associated with the presence of charge carriers greatly increases the probability of capture of low velocity electrons.

A similar series of measurements were taken on another As_2S_2 target (9291AR3). In these tests, an attempt was also made to observe the effect on the target of overnight exposure to the atmosphere of the demountable position. The solid curves of Fig. 11 give I_T as a function of I_B for 4×10^{-11} , 10^{-11} and 4×10^{-12} ampere values of input excitation. The dotted curves give the I_T vs I_B characteristic, as taken after overnight exposure in the demountable position, at 4×10^{-11} and 10^{-11} ampere levels of excitation. In general, the effect of the overnight exposure appears to be to lower the saturated signal levels somewhat, which is equivalent to lowering target gain, and to extend the saturated current plateau, which now occurs over a wider range of I_B values.

The $(1-\bar{\delta})$ curves, before and after overnight exposure in the demountable, are plotted in Figs. 12 and 13 respectively. It is interesting to note in Fig. 12 that the $(1-\bar{\delta})$ values for 4×10^{-11} and 10^{-11} ampere input excitations show the same marked increase with input excitation as was observed in the data of Fig. 10.

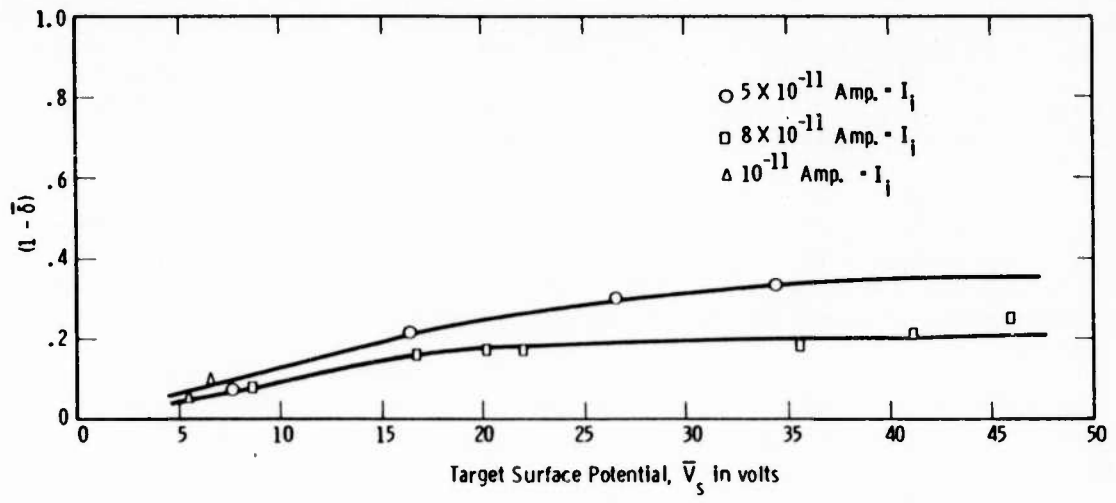


Fig. 8— Plot of $(1 - \bar{\delta})$ as function of \bar{V}_s for As_2S_2 target (target 581 AR1, $V_T = 50$ volts)

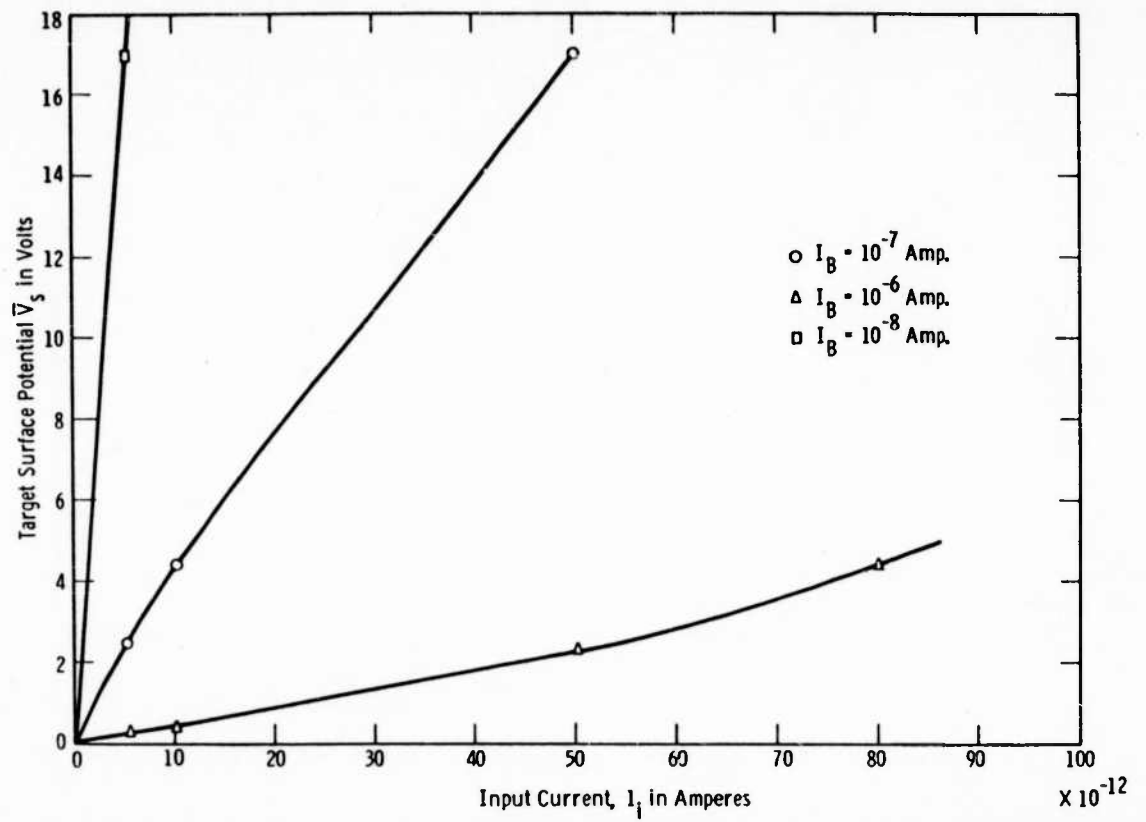


Fig. 9--Target surface potential \bar{V}_s as function of input current for $As_2 S_2$ target and different values of beam current.

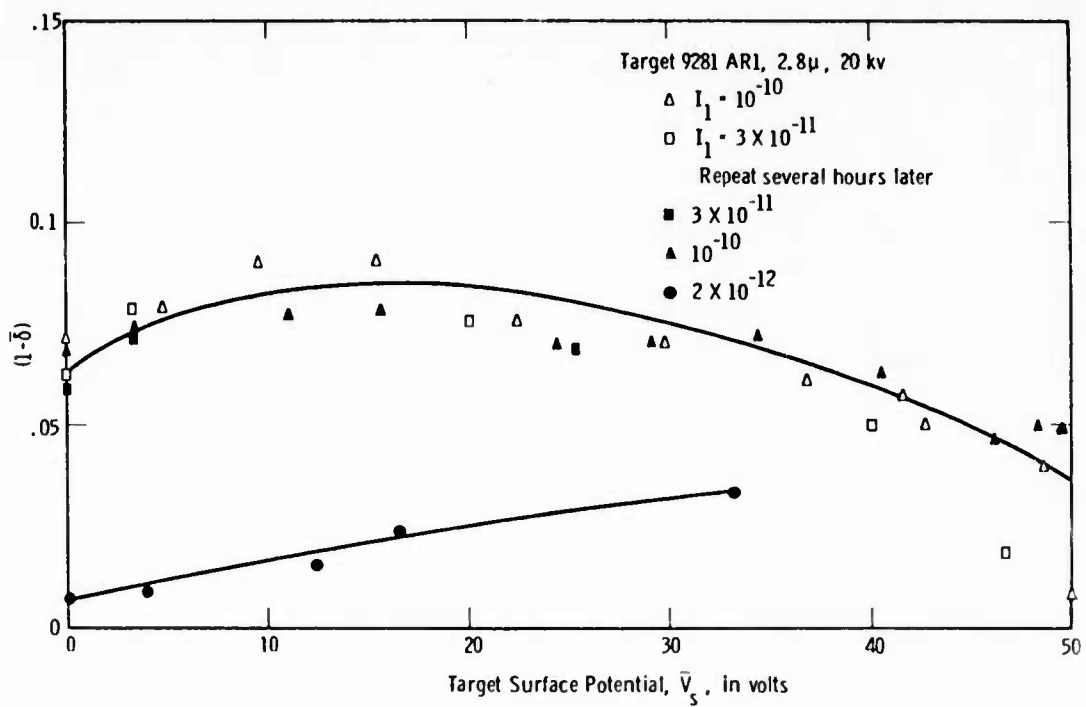


Fig. 10—Plot of $(1-\bar{\delta})$ under imaging conditions as function of \bar{V}_s for As_2S_2 target.

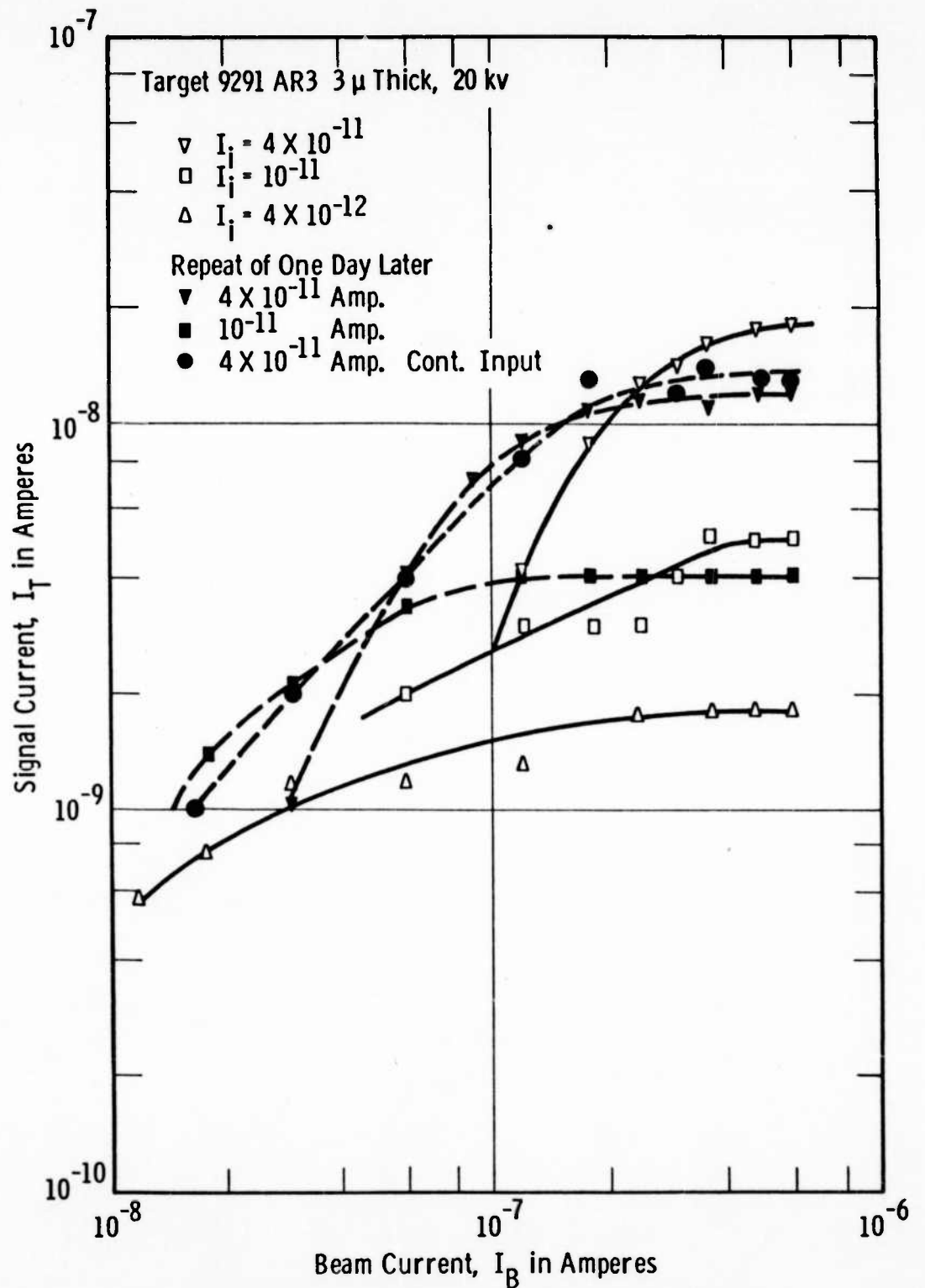


Fig. 11-EBIC signal current for As_2S_2 target as function of I_B for different values of input current.

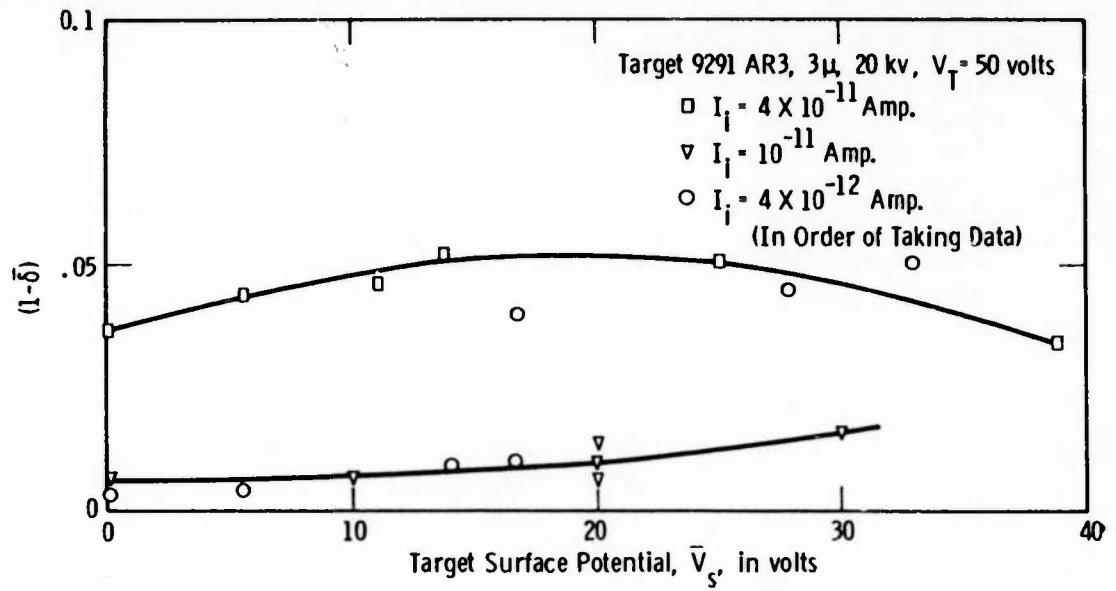


Fig. 12—Plot of $(1-\bar{\delta})$ under imaging conditions as function of \bar{V}_s for As_2S_2 target.

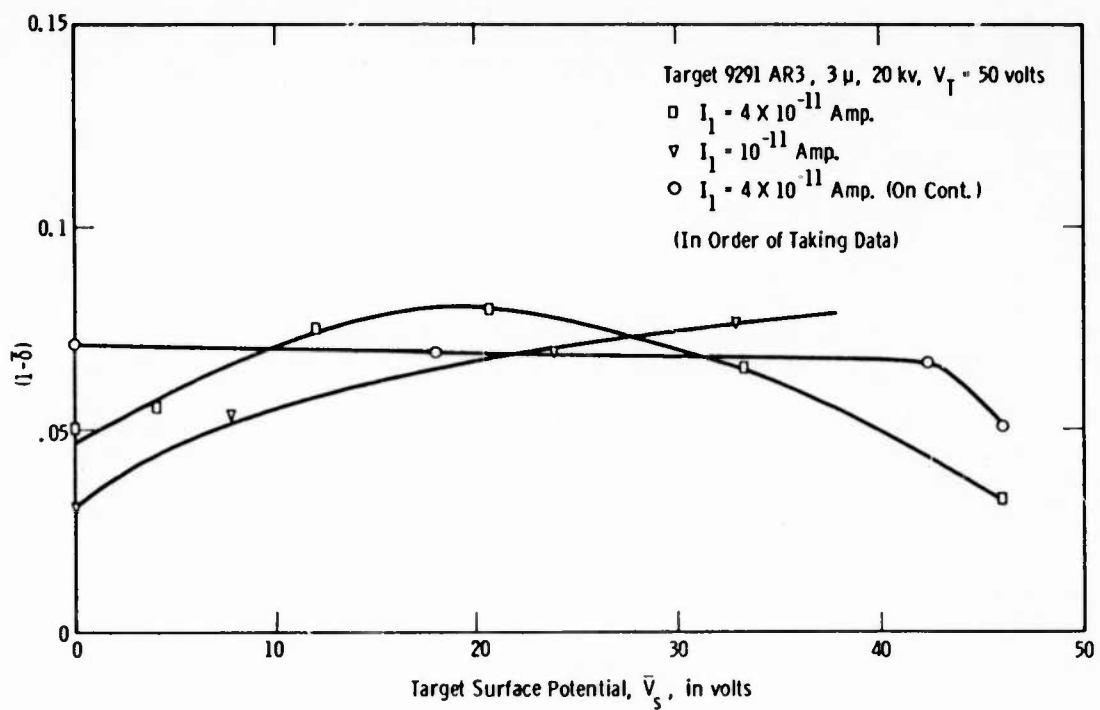


Fig. 13—Plot of (1- $\bar{\delta}$) under imaging conditions as function of \bar{V}_s for As_2S_2 target after overnight exposure in demountable.

However, the electron absorptivity curve at 4×10^{-12} ampere excitation level appears to switch from a low level to a high level of electron absorptivity while the measurements were being made.

Ordinarily, the input excitation was energized on an intermittent basis, and was interrupted as soon as a given measurement was made. A repeat 4×10^{-11} ampere curve was taken with the excitation on continuously. This curve is also shown in Fig. 11. The corresponding electron absorptivity curve, which is shown in Fig. 13, is characterized by an unusual flat response.

The $(1-\bar{\delta})$ characteristic for an As_2S_3 target (909) are given in Fig. 14 for different excitations. Two points are also given for a separate As_2S_3 target. Sufficient data have not been taken to date so as to afford a reliable criteria for assessing the electron absorptivity of As_2S_3 versus As_2S_2 . It may well be that the variation between individual targets will turn out to be large compared to the average difference in characteristics. There seems to be some indication that As_2S_3 has a higher reflectivity for low velocity electrons.

Fig. 15 gives the $(1-\bar{\delta})$ characteristics for an As_2S_2 and an As_2S_3 target having an overlayer of 0.2 microns of Sb_2S_3 . There is some indication that the overlayer has not significantly affected the electron absorptivity of the surfaces, which appear to be determined by the substrates beneath the Sb_2S_3 films.

The $(1-\bar{\delta})$ characteristics of an As_2S_2 target having a relatively thick overlay of Sb_2S_3 (0.5μ) is shown in Fig. 16. Here a substantial change in electron absorptivity with change in input excitation is noted. The curve with 3×10^{-10} ampere input has the highest electron absorptivity. The $(1-\bar{\delta})$ corresponding to 10^{-10} ampere excitation is significantly lower. The 10^{-11} ampere curve has the lowest $(1-\bar{\delta})$ values on the curve. It is interesting to note that a reversal apparently takes place, with the 5×10^{-12} ampere curve falling between the 10^{-11} ampere and the 10^{-10} ampere curves. A similar reversal took place on Fig. 8, where the electron absorptivity corresponding to an 8×10^{-11} ampere input is somewhat lower than the $1-\bar{\delta}$ corresponding to a 5×10^{-11} ampere input excitation.

The effect of evaporating an Sb_2S_3 overlayer 0.5 microns in thickness had no effect on the electron absorptivity of As_2Se_3 at 10^{-11} ampere excitation. Curves taken before and after excitation are shown in Fig. 17. However, increase in excitation to 3×10^{-10} amperes produced a substantial increase in the $(1-\bar{\delta})$ characteristic as indicated by the upper curve of the figure after evaporating of the Sb_2S_3 overlay.

For purposes of comparison, the $(1-\bar{\delta})$ characteristic was taken of a standard commercial Sb_2S_3 vidicon tube. Since the entire scanned raster area was illuminated, the $(1-\bar{\delta})$ values in Fig. 18 are "actual". From the data taken, it would appear as if the V_s corresponds to the first crossover would be in the neighborhood of 17 to 18 volts which is substantially lower than observed values

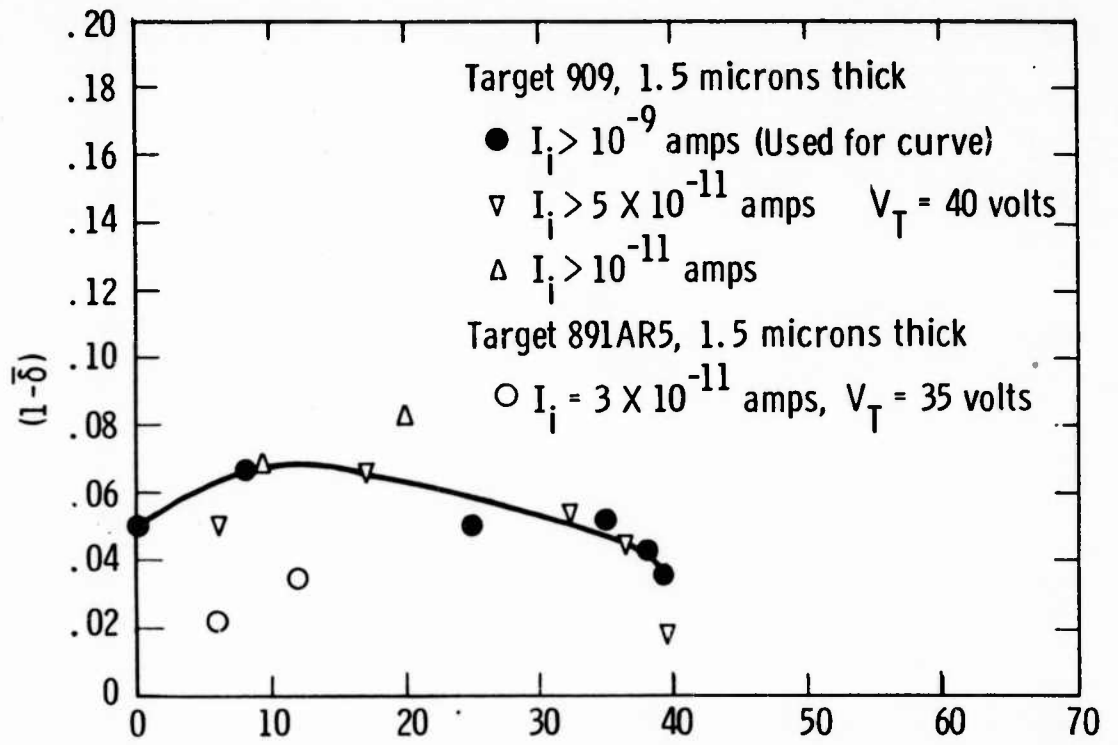


Fig.14—Plot of $1 - \bar{\delta}$ as function of \bar{V}_s for As_2S_3 targets

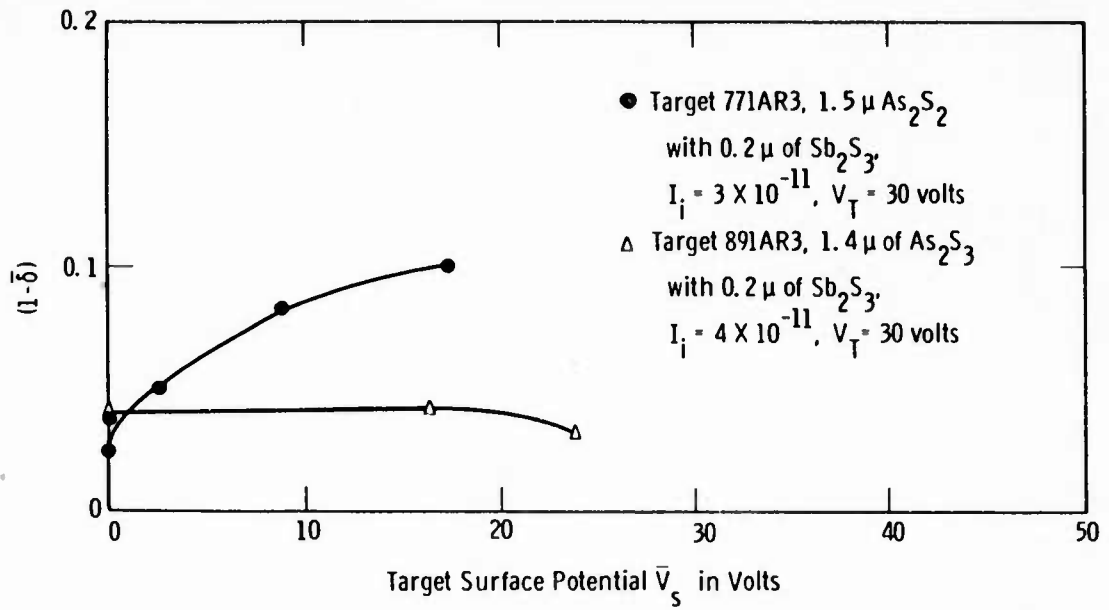


Fig. 15-Plot of $(1-\bar{\delta})$ as function of \bar{V}_s for EBIC targets with vacuum evaporated overlayer of Sb_2S_3

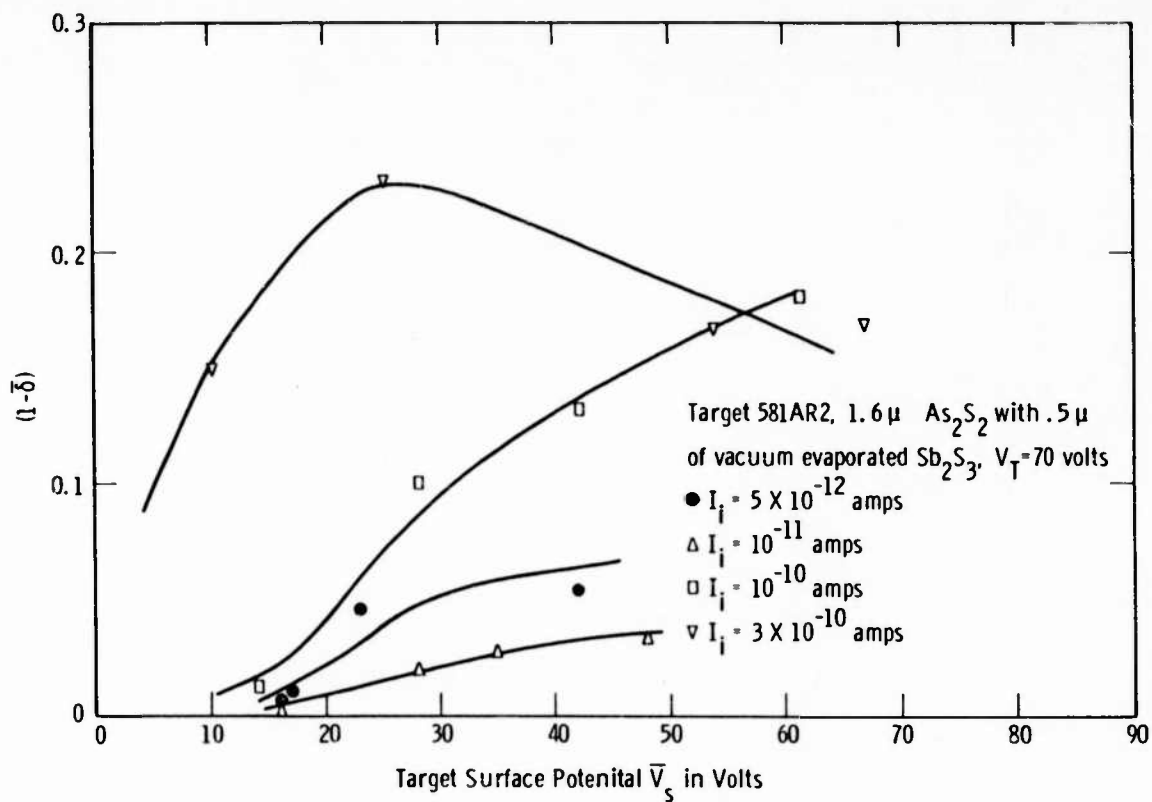


Fig. 16—Plot of $(1-\delta)$ as function of \bar{V}_s for As_2S_2 with Sb_2S_3 vacuum evaporated overlayer

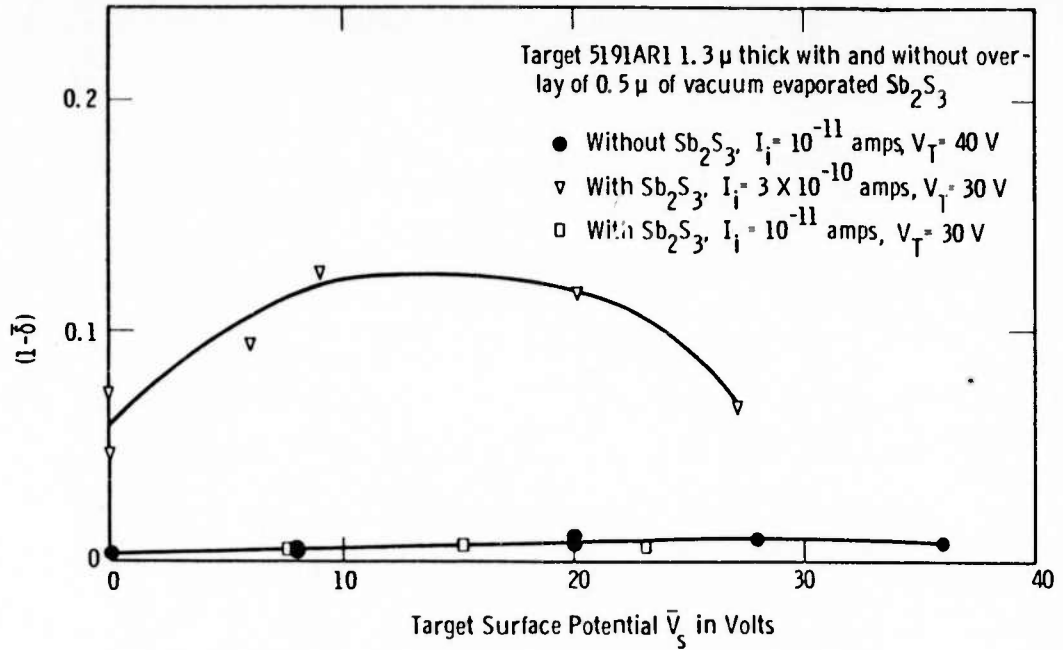


Fig. 17-Plot of (1- δ) as function of \bar{V}_s for As_2Se_3 EBIC target

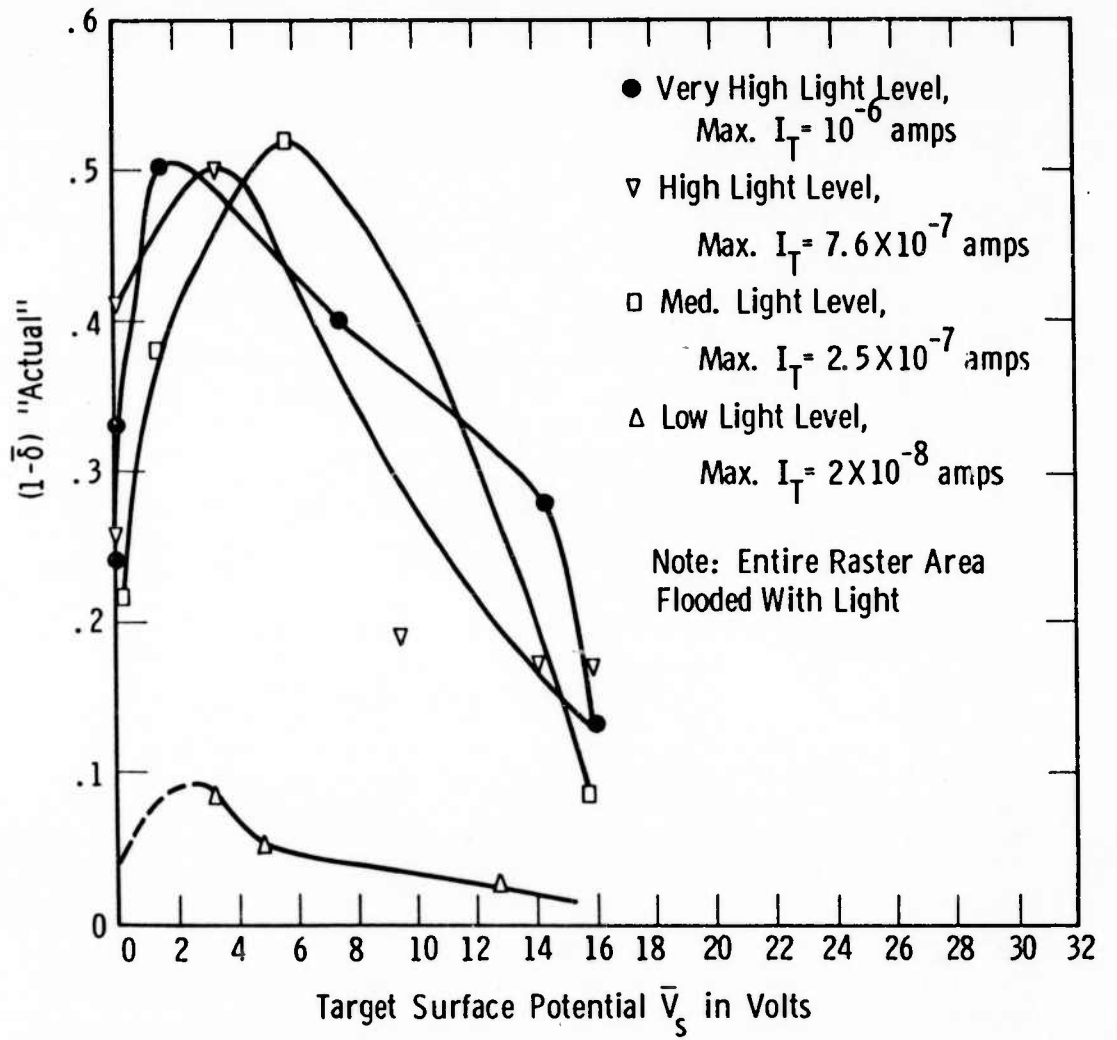


Fig. 18 - Plot of $(1-\bar{\delta})$ as function of \bar{V}_s for vidicon tube, $V_T = 16$ volts

for arsenic sulphides. It is interesting to note that the $(1-\bar{\delta})$ value corresponding to a low input illumination was very low, again indicating very high reflectivity for low velocity electrons at low values of excitation.

In general, the first crossover potential for As_2S_3 and As_2S_2 has usually been between 50 and 90 volts. One of the techniques for determining the first crossover potential has involved exposing the target to a bright light with the beam off at a given test value of backplate potential. The scan beam is then energized suddenly, and the video pattern on the monitor observed to determine whether any parts of the raster have gone over the first crossover potential. By extrapolation, the curves of Figs. 10, 12, 13, 14, and 15 appear to have first crossover potential in the range determined by these independent monitor observations.

It is interesting to note that the deposition of relatively thick layers of Sb_2S_3 over the arsenic sulphides have not significantly affected the first crossover potential, which is apparently determined by the characteristics of the substrate layers.

Evidently it would be possible to obtain a video image from the target of Fig. 16, even if all parts of the target surface were at a common value of \bar{V} . The state of excitation of the target acts in a manner similar to a grid, essentially reflecting electrons from dark areas of the target, and interfering with the reflection, i.e., absorbing more of the electrons which are attempting to leave signal areas, in proportion to the signal excitation. It is this mode of image which was referred to previously as charge carrier beam modulation imaging.

Curves of I_T versus V_T for an As_2S_2 target (9181AR2) have been plotted in Fig. 19 for input excitations of 3×10^{-11} , 10^{-11} , and 3×10^{-12} amperes. It is important to know in interpreting the results whether the curve corresponding to 3×10^{-11} amperes input represents saturated values of beam input current. I_T versus I_B curves taken at $V_T = 20$ and 50 volts have established that the 3×10^{-11} ampere input excitation curve represents saturated values of I_T in the I_T vs I_B curve to backplate potentials of at least 50 volts.

From these curves it is evident that the approximation made by assuming that the target responds ohmically (i.e., would exhibit a linear response in Fig. 19) introduces no very great error for As_2S_2 targets having up to 50 volts impressed across them.

The signal current curves of Fig. 19 which correspond to 3×10^{-11} and 10^{-11} ampere excitations vary with 1.1 and 1.5 power respectively of the applied backplate voltage. The upper part of the 3×10^{-12} ampere excitation curves varies with the 3.2 power of the backplate potential. The characteristics of the target of Fig. 19 fall into the general pattern described by Lampert, Ref. 7, for an insulator with traps. The higher than unity power variation of I_T vs V_T is due to an increase in Fermi level of the solid as the trapping states get filled. Further confirmation that the I_T vs V_T characteristics are affected by the presence of traps are the high transient signals noted when target voltage is suddenly increased during EBIC excitation. Similar transients have been noted in CdS

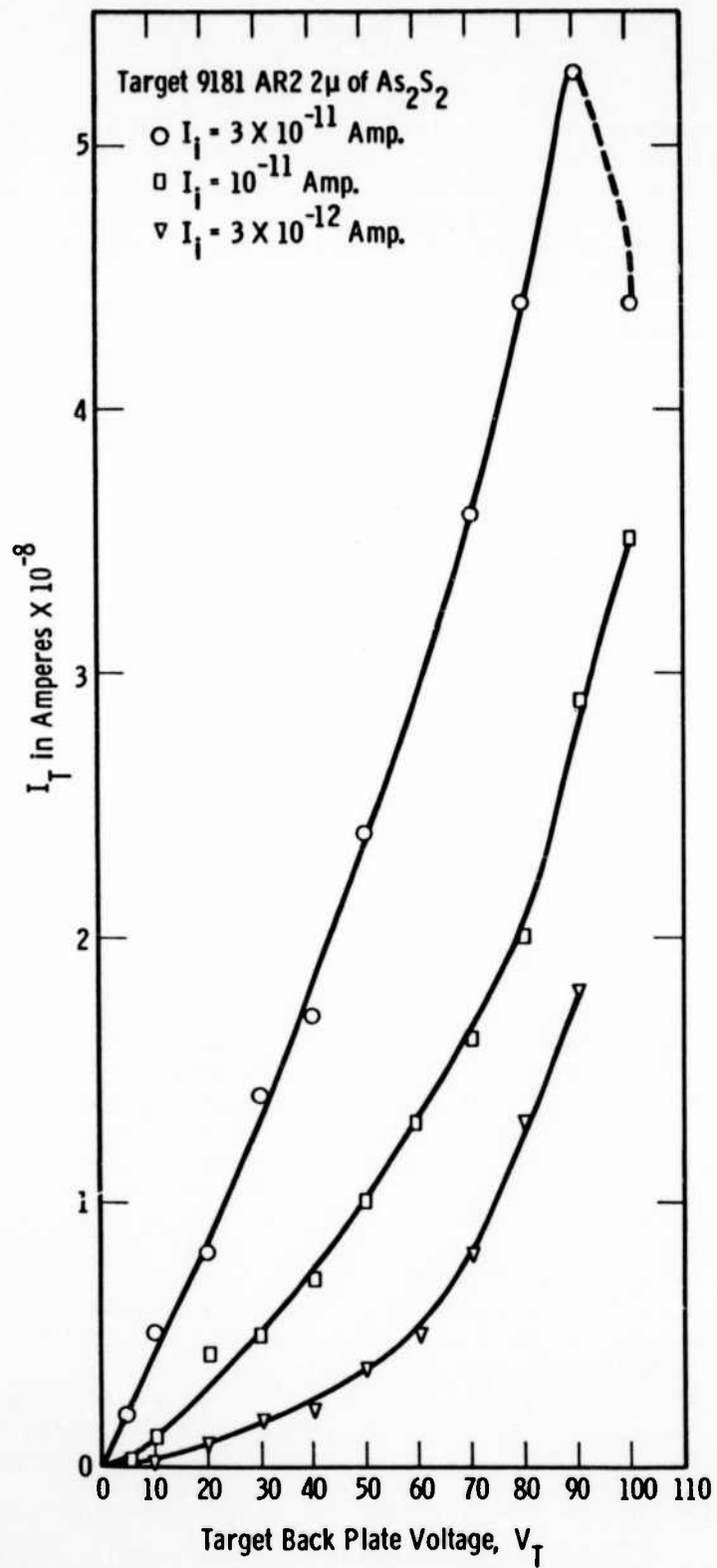


Fig. 19 $-I_T$ versus V_T for $I_B = 10^{-6}$ Amp. and different input currents.

crystals by Smith and Rose, Ref. 8. These authors explain the transients as due to surges of charge carriers which are injected into the insulator from the contacts and which are capable of passing relatively high currents before a good portion of the excess charge gets trapped. The presence of filled traps increases the density of space charge within the solid, thereby limiting the flow of charge to steady state values which are very small compared to the steady state currents attainable in a trap-free solid.

Similar curves to those of Fig. 19 are plotted in Fig. 20 using a factor of 10 lower beam. The beam employed is not large enough to insure signal current saturation at the higher signal current levels, and the secondary emission characteristics of the target play a significant role in determining the shape of these curves. The 10^{-11} and 3×10^{-12} amperes input curves are higher at low values of V_T than the corresponding curves for the higher beam. This may be due to a change of characteristics of the material with continued excitation or to experimental difficulties.

The effect of beam current level on the I_T vs I_1 characteristics of an As_2S_2 target are shown in Fig. 21. A similar plot on a log-log scale is given in Fig. 22 for a separate, somewhat thicker, As_2S_2 target. The curve corresponding to the highest value of beam in this figure has a 0.9 power variation of signal current relative to input current.

It is interesting to note that the curves corresponding to the lower value of beam currents rise to maximum values and then start to decrease. It would appear that these maxima do not correspond to space charge limited current saturation values but rather are ascribable to values of \bar{V}_S which have exceeded the maxima on the curves of \bar{V}_S vs $(1-\delta)$.

c. Discussion on Electron Absorptivity of Insulators

Unless energy absorbing collisions occur within an insulator, one would expect that low velocity electrons impinging on a surface will eventually experience a series of elastic reflections which will cause them eventually to leave the solid. Further, it would be necessary, if the electrons are to be retained within the solid in the case of inelastic collisions, that they lose enough energy per collision so that they do not have enough energy to overcome the electron affinity of the surface should they reach the surface in the course of their motion. Since the mechanisms of energy loss for secondary electrons leaving an insulator from a site a number of hundred Angstroms beneath the surface have much in common with energy losses experienced by low velocity scan electrons entering the material, the energy losses experienced by secondary electrons which originate within the volume of a material on their way out of the solid are very pertinent to the problem at hand.

The high secondary emission yield from insulators has been explained, Ref. 9, as due to an increased depth of escape of secondary electrons. The larger

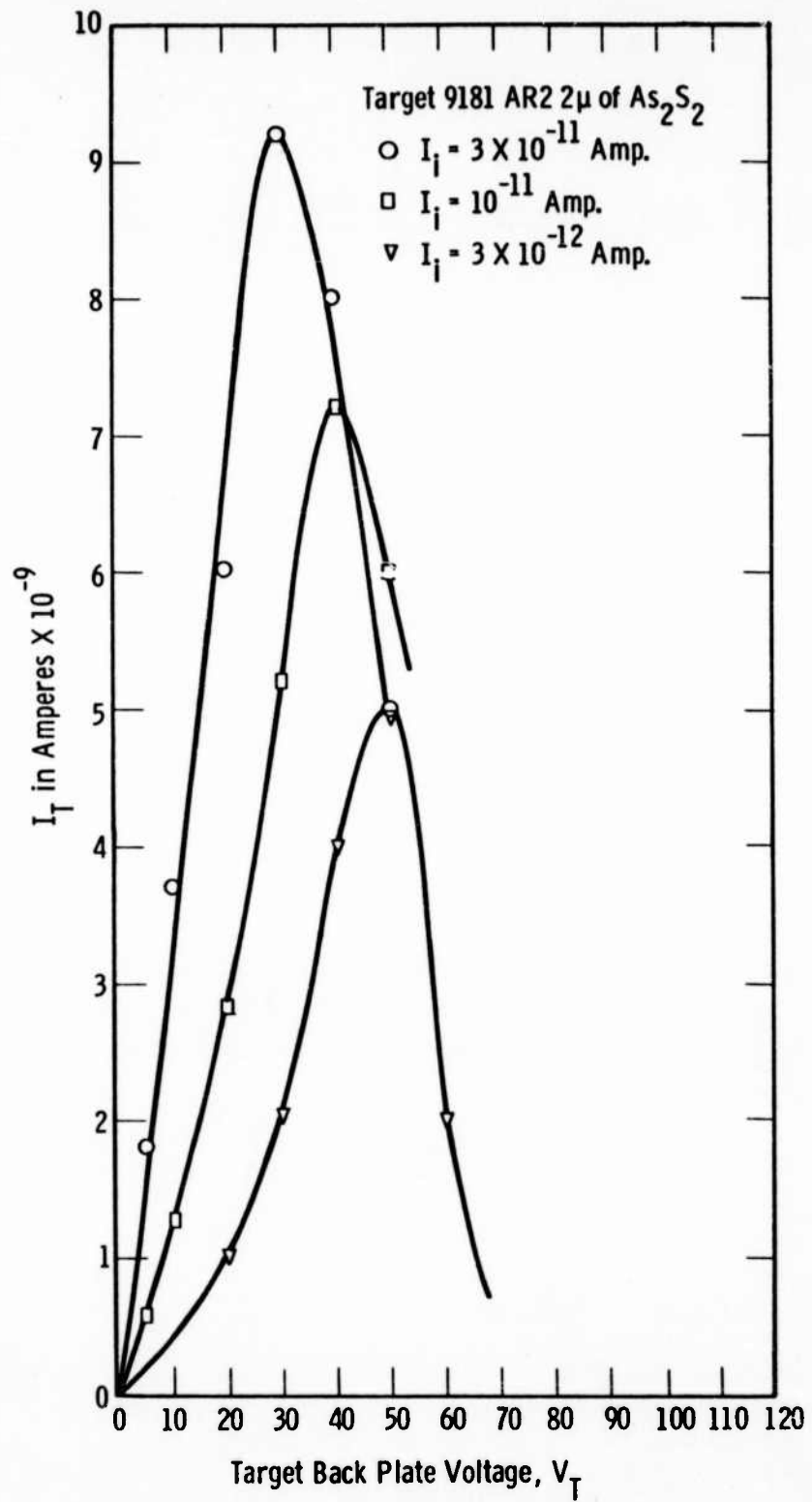


Fig. 20 - I_T versus V_T for $I_B = 10^{-7}$ Amp. and different input currents.

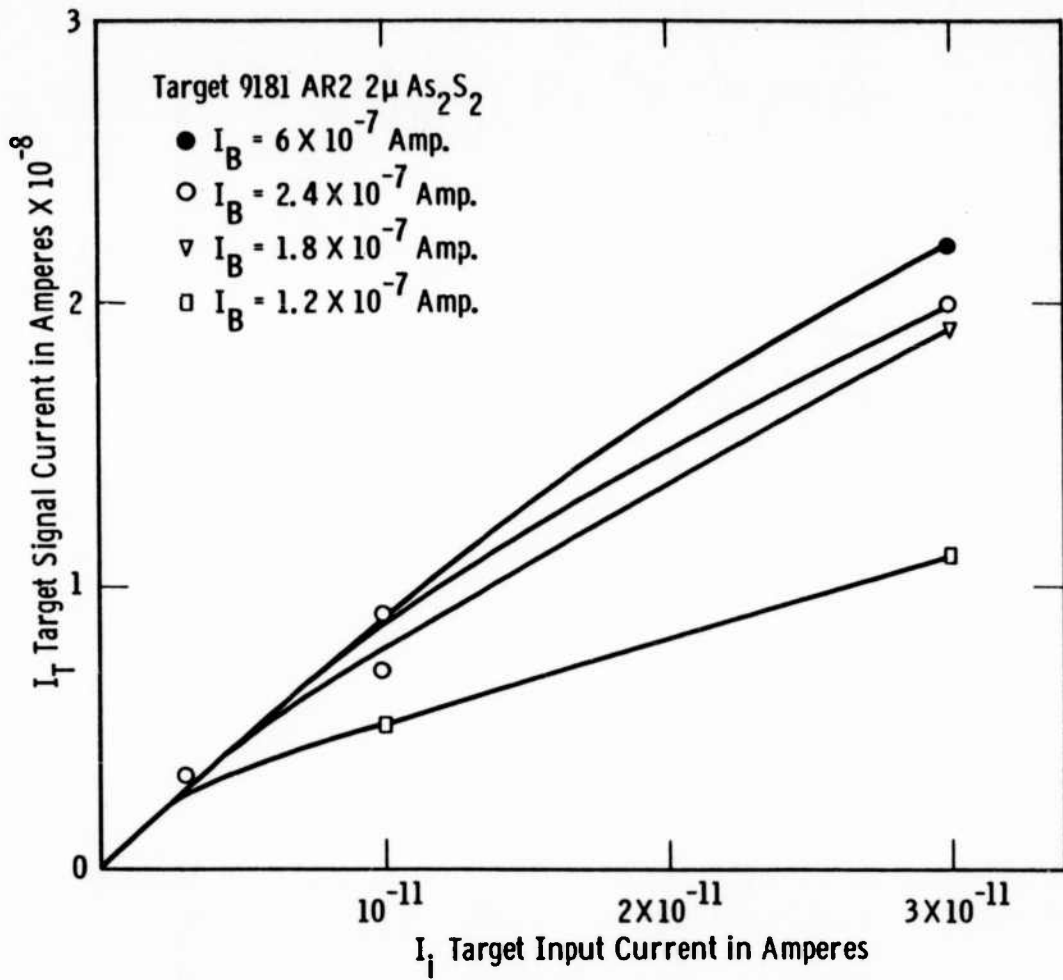


Fig. 21 -Target signal vs. input current for different values of I_B and $V_T = 50$ volts

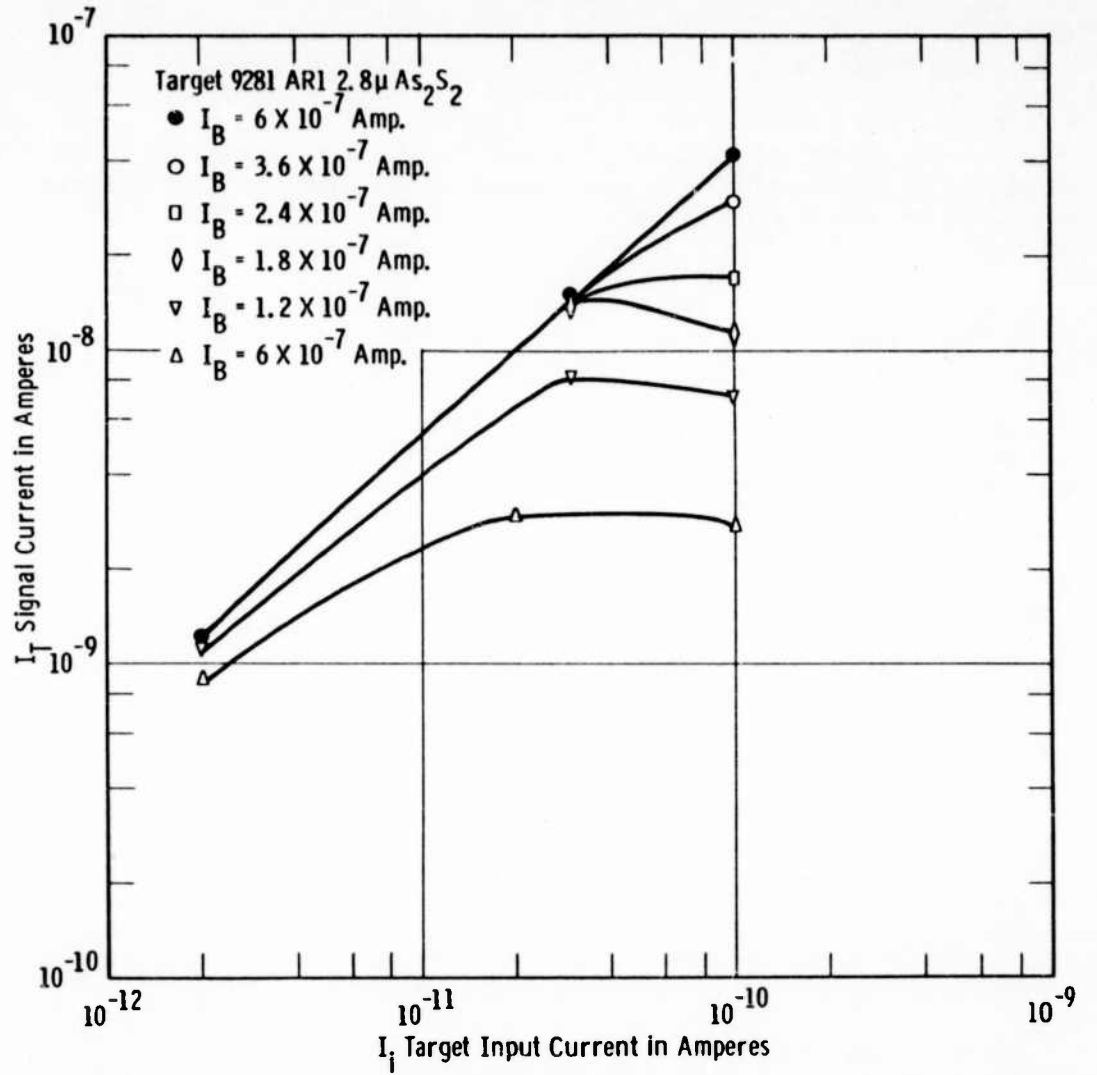


Fig. 22 —Target signal vs. input current for different values of I_B and $V_T = 50$ volts

mean free path for electrons in an insulator is attributable to a lower probability for collisions which involve energy losses.

One of the commonly held theories of secondary emission from metals holds that the secondaries which are released within the volume lose their energy rapidly by interaction with the conduction electrons. This mechanism for absorption of energy from electrons does not occur within insulators because of the low density of charge carriers. The following are the principle mechanisms, Ref. 9, for absorption of energy from low energy electrons by insulators: (1) electron-phonon interaction, i.e., interaction with lattice vibrations, (2) interaction with valence electrons, i.e., creation of electron hole pairs, and (3) interaction with lattice defects.

Dekker, Ref. 10, has estimated the depth of escape of secondaries from Pt, Ge, and MgO as corresponding to 20, 35, and 230 A respectively. Haxby, Ref. 11, has experimentally determined that secondary electrons can be released in MgO films from depths of the order of 400 A. The depths cited above for insulators are very low compared to the thickness of Sb_2S_3 overlays discussed in the previous section.

The salient question as to the distances which can be traversed by electrons in an insulator of course has to do with the mechanism for absorption of energy of the electron within the insulator in question. If the electron has insufficient energy to produce band-to-band transitions, then it would appear that relatively large ranges are possible with certain materials. In work on selenium, Ref. 4, 16, it has been demonstrated that the range of carriers can be of the order of 5 to 10 microns. Similarly, it has been possible to obtain relatively high EBIC gains in As_2S_2 films which are of the order of 4 μ thick. Since the primary electrons are absorbed in less than 2 μ of thickness, it is evident that the range of carriers is at least of the order of 2 μ for As_2S_2 . In order for the electrons to escape from the material, they must reach the surface with sufficient energy to overcome the electron affinity of the surface, which conceivably could be as low as 0.5 ev, and even lower.

Several experiments, Ref. 12, 13, have demonstrated that electrons can be trapped in KCl films and then released by bombarding electrons having initial energies in the same range as the equivalent photon interactions, Ref. 14. Jacobs, Martin, and Brand, Ref. 14, working on composite surfaces have concluded that true secondaries originate from the filled band, i.e., transitions across the band gap of the insulator, rather than from traps.

These experimenters, Ref. 14, show experimental curves in the range between 0 and 20 ev which are relevant to the measurements made in the previous section. For an AgCsO film, the secondary emission ratio for primaries between 2 and 10 ev is of the order of .96 to .98, corresponding to "actual" (1- $\bar{5}$) of the order of .02 to .04. The secondary emission ratio of KCl dips to a minimum of .955 at 9 ev. Both of these materials show the very high electron reflectivity for low velocity electrons noted in the previous section. In general the

threshold values for secondary emission check closely with the optical energies required to remove an electron from the filled band into the vacuum.

Fredericks and Cook, Ref. 15, in similar measurements on KCl have determined electron absorptivity values between .2 and .3 in the range of electron energies between 1 and 10 ev. Somewhat lower absorptions were determined for KBr. The KCl absorptivity data are in disagreement with the work of Ref. 14.

Referring to the change in $(1-\bar{\delta})$ as a function of input excitation observed in the previous section, it is likely that this effect can be explained on the basis of increased opportunities for the absorption of the energy of low velocity electrons by electrons in filled traps rather than by direct interaction with the charge carriers. Further careful measurements are required to help understand the mechanism, and to determine the applicability of the effect to the imaging problems at hand.

4) Survey of EBIC Target Materials*

a. Arsenic Compounds of the $M_2^{VB} X^{VIB}$ Family

Table II summarizes the EBIC characteristics of a number of different formulations of As, Se, and S, as substituted in the basic As_2S_3 and As_2Se_3 stoichiometry. From this table it is evident that the EBIC gain tends to increase as the percentage of selenium employed in the material increases. Vacuum baking of the experimental targets for 2 hrs at $100^\circ C$ did not produce very substantial changes in the EBIC gain. The vacuum bakes did substantially decrease the persistence of the As_2Se_2S and As_2SeS_2 targets, and tended to increase the number of bright spots in the dark current image.

In the preliminary tests most of these materials exhibited an ohmic variation of signal current with target voltage and a first power variation of output with input current at low target voltages. Persistence at a given target voltage was proportional to the duration and magnitude of the excitation current. The persistence of As_2Se_2S targets generally increased with target voltage, whereas most of the other materials listed in Table II either exhibited small change in persistence with change in target voltage, or the persistence decreased with increasing target voltage.

In general, the ability to operate at high target voltages was limited by the appearance of a large array of target spots as target voltage was increased, and by the tendency of the surface to go over the first crossover potential.

The formulation As_2Te_2S was also tested. No EBIC image was obtained.

* Most of the special materials were made in the Semiconductor Department under the guidance of Dr. A. Cornish.

TABLE II
EBIC CHARACTERISTICS OF SOME STOICHIOMETRIC
FORMULATIONS OF As, Se AND S

Target No.	Mat.	Approx. Thickness (Microns)	Gain	V_T	Seconds Persistence	
					High Level	Low Level
L630	As_2Se_2S	3	1200	40	15	60
L633	"	3	600	40	4	12
L636	"	1.7	1050	50	long	
L637	"	1.7	700	40	5	long
L635	"	1.7	500	40	long	
	(after 2 hr 100°C bake)		800	30	3	
L638	As_2SeS_2	2.2	900	40	long	
	(after 2 hr 100°C bake)		800	40	4	
L639	As_2Se_2S	2.2	700	50	15	long
	(after 2 hr 100°C bake)		600	40	4	
L640	As_2Se_2S	2.2	400	30	7	
	(after 2 hr 100°C bake)		500	40	5	
L641	As_2Se_2S	1.7	900	50	4	16
L643	"	1.7	900	50	long	
	(after 2 hr 100°C bake)		600	40	6	
L688	$As_2Se_{2.5}S_{0.5}$	2.6	1000	30	3	
L689	"	2.6	1500	40	1	long
L690	"	2.6	900	30	4	
L692	$As_2Se_{1.5}S_{1.5}$	3.5	800	50	5	
L694	"	3.5	500	40	4	10
L695	"	3.5	700	50	2	long

Preliminary tests on non-stoichiometric formulations of As, Se, and S are shown in Table III. These materials have tended to be more persistent than the materials listed in Table II. All of these materials increased in persistence as a function of backplate potential.

A two section evaporation of Sb_2S_3 was superimposed on target L773. One-third of the area of the target consisted of an $As_2Se_2S_{0.5}$ film having about a 1μ layer of Sb_2S_3 over it, a second area had a $.5 \mu$ coating of Sb_2S_3 evaporated onto it. The remaining area of $As_2Se_2S_{0.5}$ was shielded from the Sb_2S_3 layer during the evaporation. As the target backplate voltage was increased, target bright spots first showed up in the area which had been shielded from Sb_2S_3 during the evaporation. This area was also the first area which exhibited first crossover difficulties. In general there appeared to be no advantage associated with the use of targets having off-stoichiometric formulations.

The substitution of oxygen for one of the sulphur or selenium atoms in the As_2S_3 stoichiometry tended to lower the EBIC gain somewhat. Such targets were also limited in the backplate potentials at which they could be operated by the presence of bright spots. Results on these targets are summarized in Table IV. Also shown in this table are test results on two formulations in which one arsenic atom is replaced by an Sb atom. Gains in both $AsSbS_3$ and $AsSbSe_3$ were lower than most of the other formulations summarized in Tables II, III, and IV.

b. Ternary Formulations Incorporating As and Se

Certain metals of the IIB group of the periodic table form compounds with Se and S such as ZnSe and CdS, which are stable at high temperatures and which have low vapor pressures. These materials are capable, when properly activated, of giving good photoconductive response. For this reason it appeared to be appropriate to investigate whether ternary materials incorporating Se and As and metals such as Zn and Cd would have useful EBIC characteristics as well as better stability with temperature.

Test results on $CdAs_2Se_4$, which are summarized in Table V, indicate capabilities of high EBIC gains at relatively low values of target backplate voltages. Persistences were initially excessive, but decreased when the material was vacuum baked for 2 hrs at $100^\circ C$. Substantially higher filament currents were required to evaporate the $CdAs_2Se_4$ material. In view of some evidence of decomposition during evaporation, a chemical analysis of the evaporated film was made. The ratio of Se to As exactly corresponded to that expected from As_2Se_3 . The indications are that the following reaction takes place under vacuum when the temperature gets sufficiently high:



Since the CdSe has a low vapor pressure, relatively little of it would be expected to reach the EBIC film.

TABLE III

EBIC CHARACTERISTICS OF SOME NON-
STOICHIOMETRIC FORMULATIONS OF As, Se AND S

Target No.	Mat.	Approx. Thickness (Microns)	Gain	V_T	Seconds Persistence	
					High Level	Low Level
L763	$As_2Se_{1.5}S$	2.5	1300	50	60	long
L767	$As_{1.5}S_2S$	1.3	700	50	long	
L768	"	1.3	800	40	5	
L773	$As_2Se_2S_{0.5}$	1.4	1100	50	long	
					after evaporation of a Sb_2S_3 double layer	
			2200	75	long	
			1000	30	1	

TABLE IV
 EBIC CHARACTERISTICS OF SOME SPECIAL
 FORMULATIONS OF As, Se, S AND O

Target No.	Mat.	Approx. Thickness (Microns)	Gain	V _T	Seconds Persistence	
					High Level	Low Level
L710	As ₂ S ₂ O	1	400	50	2	12
L746	"	2.5	200	50	3	25
L704	As ₂ SeSO	1.1	100	20	22	long
L705	"	1.1	400	30	3	
L706	"	1.1	400	30	2	
L750	"	1.5	400	30	9	
L755	AsSbS ₃	.07	(no image or gain)			
L758	"	.8	330	40	long	
L761	AsSbSe ₃	.05	270	20	4	25
L782	"	1.3	(no image)			

TABLE V
EBIC CHARACTERISTICS OF CdAs₂Se₄

Target No.	Mat.	Est. ug/cm ²	Gain	V _T	Seconds Persistence		
					High Level	Low Level	
L855	CdAs ₂ Se ₄	330	600	20	long		
L864	"	615	1700	30	"		
L865	"	615	650	15	long		
			1500	35	"		
			After 2 hr 100°C bake	1000	40	1	
L866	"	615	400	8	1/2	60	
			700	15	long		
L868	"	615	1000	8	long		
L929	"	615 (In substrate)	After 2 hr 100°C bake	1666	50	1/2	30
			"	300	10	1/2	
4271AR2	"	254	200	10	2		
4271AR6	"	254	500	20	1/2		
4251AR1	"	351	500	25	long		
L928	"	about 1000		1250	40	long	
			After 2 hr 100°C	1200	30	1	long
			(add 105 ug/cm ² Sb ₂ S ₃)	2200	40	1/2	long

The highest gain using the CdAs_2Se_4 material was observed on a baked film (L928) after approximately a $.2 \mu$ layer of Sb_2S_3 was evaporated over it. A gain of 2200 was observed at 40 volts.

Test results on several other ternary materials are summarized in Table VI. AgAsSe_2 exhibited low gain at low target thickness, but improved with thickness. Targets fabricated of ZnIn_2Se_4 were capable of reverse polarity images only, whereas targets fabricated of ZnAs_2Se_4 , CdAs_4Se_7 and HgAs_2Se_4 had promising gains. The AgAsSe_2 material revealed only a trace of Ag present in the evaporated target according to spectrographic tests. The indications are that the target materials resulting from the evaporation of the materials in Table VI are probably largely As_2Se_3 with some impurities present.

The type of substrates used appears to be of considerable importance with some of the materials employed. All of the targets listed in Table V made use of Al substrates which were evaporated onto Al_2O_3 self-supporting layers as described in Ref. 1, with the exception of target L828 which made use of an In substrate. Several CdAs_2Se_4 targets, not listed in the table, which were evaporated onto gold substrates exhibited no gain although some imaging was possible.

Similar results were observed in the tests on AgAsSe_2 targets. When 115 ug/cm^2 of this material was evaporated onto 3 targets having indium, gold, and platinum substrates, these targets were incapable of imaging even through companion targets having Al substrates and subject to the same evaporation, did exhibit gain and imaging capabilities. The evaporation of a second layer of AgAsSe_2 improved the target with the gold substrate to the extent that a gain of 670 was obtained at 5 target volts. The platinum substrate target which was also subjected to a second evaporation was still incapable of imaging.

c. Summary of Sb_2S_3 Type Materials

Tests on Sb_2S_3 type materials are summarized in Table VII. In general, Sb_2S_3 targets exhibit higher gain under reverse polarity scan conditions. Targets in which the initial material was 50% Sb_2S_3 and 50% As_2S_3 have promising gains under conditions of normal polarity scan. Both Sb_2SO_2 and $\text{Sb}_2\text{S}_2\text{O}$ also appear to be promising in terms of the gains observed at low target voltages.

By the use of a rotatable shield it was possible to evaporate the Sb_2S_3 on target L791 in layers having 3 different thicknesses varying from $.3 \mu$ for the thinnest, to $.7 \mu$ for the intermediate layer, and 1.2μ for the thickest evaporation. In general the $.3 \mu$ section was useable at low target voltages only. The 1.2μ thick area had the best EBIC performance from the standpoint of imaging at the low input currents. This layer also had less bright spots at a given target voltage.

Several Sb_2Se_3 targets were also checked. No gain was observed, apparently because of the high conductivity of this material.

TABLE VI

EBIC CHARACTERISTICS OF TERNARY
MATERIALS INCORPORATING SELENIUM

Target No.	Mat.	Est. ug/cm ²	Gain	V _T	Seconds Persistence	
					High Level	Low Level
L842	AgAsSe ₂	283	500	20	1	long
L849	"	115	250	10	8	
L850	"	115	175	20	8	
L851	"	115	166	10	5	
L857	" approx.	(500)	1000	20	long	
L822	ZnIn ₂ Se ₄	210	(dim reverse polarity image)			
L915	ZnAs ₂ Se ₄	367	320	20	3	
L996	CdAs ₄ Se ₇	323	500	20	1	10
L998	"	323	500	20	long	
4211A1	HgAs ₂ Se ₄	238	500	20	15	

TABLE VII
 EBIC CHARACTERISTICS OF Sb_2S_3 TYPE MATERIALS

Target No.	Mat.	Est. 2 ug/cm	Gain	V_T	Seconds Persistence	
					High Level	Low Level
L342	Sb_2S_3	730	40	10	13	
			300	170*	4	
L344	"	730	500	190*	9	
L791	Sb_2S_3	Triple Layer	300 Low Gain*	10 30-200	5	
L901	"	420	no gain			
L950	$1/2 Sb_2S_3$	330	575	40	1	long
	$1/2 As_2S_3$ (after 2 hr 100°C)		470	50	1/2	8
L951	"	330	750	50		long
L953	"	330	550	50	1/2	3
L879	Sb_2SO_2	413	500	15	long	
L881	Sb_2S_2O	300	100	8	11	

* Reverse Polarity Scan

d. Alkali Halides

Several alkali halide materials not previously investigated have been tested. NaCl, LiI, and KBr did not demonstrate appreciable gain, although these materials evidenced the capability for EBIC imaging. Experimental NaI and KI targets without thallium activators exhibited approximately the same performance.

e. Miscellaneous Materials

1. $Cd_3As_4Se_6As_2O_3$

Several targets were fabricated of this material. In general the targets were too thin for good performance (175 ug/cm^2). However, a gain of 250 at 10 volts was obtained on one of the targets.

2. GaP, Al_2Te_3 and Ga_2Se_3

The band gaps of GaP, Al_2Te_3 and Ga_2Se_3 are 2.24 ev, 2.5 ev, and 1.9 ev respectively. A 60 ug/cm^2 film of GaP gave no indication of light or EBIC sensitivity.

An Al_2Te_3 target about 80 ug/cm^2 in thickness exhibited no EBIC or light sensitivity, whereas a dim EBIC image was obtainable on a second target of the same thickness at target voltages which could be varied from 2 to 200 volts.

A 460 ug/cm^2 thickness of Ga_2Se_3 evidenced good light sensitivities. A dim EBIC image of normal polarity image could then be seen to 200 target volts.

5) Tube Program

a. Introduction

Four tubes have been manufactured under this contract. A summary of the details of these tubes is given in Table VIII. As pointed out in this table, all tubes feature vidicon scan, that is, a vidicon gun with direct target readout. Both electrostatic and magnetic image sections are used. Tubes having a magnetic image section also feature a flip-over photocathode $7/8$ " in diameter. The electrostatic sections, however, have a standard 2" diameter photocathode. The magnetic image section has a set of 17 kovar flanges, separated by 16 ceramic wafers. A linearly increasing potential is applied across the set of kovar flanges. With such an arrangement, field emission is less of a problem, since high electric field gradients are avoided.

b. Tube E-I

Tube E-I gave an unsatisfactory picture. It is believed that excessive cesium deposits on the target caused high lateral target leakage. The tube was

TABLE VIII

SUMMARY OF CONSTRUCTION DETAILS OF EBICON TUBES

Tube No.	Type of Scan	Image Section	Target Material	Target Diameter	Test Results
E-I	Vidicon	Electrostatic	As ₂ S ₃	7/16"	Poor. Excessive target fatigue.
E-II	Vidicon	Magnetic; flip-over photocathode	As ₂ S ₃	7/16"	Good. Results given herein.
E-III	Vidicon	Magnetic; flip-over photocathode	As ₂ S ₃	7/16"	Good. Results given herein.
E-IV	Vidicon	Electrostatic	As ₂ S ₂	7/16"	Initially good. Results given herein.

incapable of storing a picture in the conventional manner, and it could not integrate a picture at low light levels. Furthermore, the target had a pronounced fatigue effect, in which the target sensitivity decreased as EBIC bombardment proceeded. In addition, the connections to the photocathode and to the target were imperfect; the result was an image which fluctuated continuously with time. Resolution was low, apparently as a result of the cesium deposition. For these reasons, no quantitative data were taken on this tube.

c. Tube E-II

Tube E-II made use of a magnetically focused image section, a 7/16" diameter target and vidicon scan. Its imaging performance was quite good. The tube was operated at magnetic field strengths near 100 gauss, and at image section voltages near 20 KV, giving picture quality similar to that obtainable on an ordinary camera pick-up tube. Fig. 23 gives a set of two photographs. Fig. 23a is taken at an input illumination of 8.7×10^{-4} ft-candles, with the target overscanned. The resolution is about 600 TV lines per inch. The lower photograph represents the target underscanned at maximum resolution. The light level is about 10^{-2} ft-candles, and the resolution visible on the original photograph is 1100 TV lines/inch. On the monitor, the limiting resolution in one direction only is about 1300 TV lines/inch at the center of the tube. The resolution characteristic, showing the number of TV lines per inch as a function of input illumination, is given in Fig. 24. In obtaining these data, the tube was operated at 17 KV, with 50 volts on the target. At manufacturing date, the photocathode sensitivity was 29 microamperes per lumen. Fifteen weeks later, the photocathode sensitivity had dropped to 15 microamperes per lumen. The data taken in Fig. 24 were obtained approximately ten weeks after the tube was manufactured. As shown in that figure, the best threshold was 4.5×10^{-6} ft-candles. The tube was operable at 20 KV, but there appeared to be little added value in operating at this potential.

For the conditions represented in Fig. 23, 7 to 8 shades of gray were visible. The persistence was only fair however, since even at high light levels, it took several seconds for the image to disappear. When the target voltage was raised to 50 volts after operation at a lower voltage, some of the previous information would show up on the target for a short time. This was true for images which were allowed to remain on the target for long periods of time.

During operation of the tube at 20 KV, the tube experienced a high-voltage breakdown, which was observable on the monitor and which persisted for an hour thereafter, even when the tube was operated as low as 15 KV. The socket surrounding the kovar flanges prevented any visible determination of the exact location of the breakdown. Subsequently this effect disappeared.

After several days operation, the target was considerably slower in response than it had been initially. In fact, at a light level of 8×10^{-4} ft-candles, it was about 600 seconds before the gain had risen to 100, gain being here defined as the ratio of the target signal current to the photocathode current.

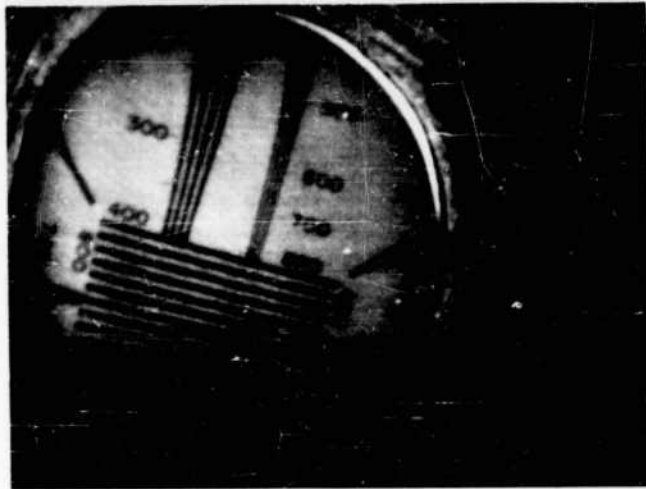


Fig. 23-a - Resolution 600 TV lines/inch at an input illumination of 8.7×10^{-4} ft-candles. Target is overscanned in this photograph.



Fig. 23-b - Resolution on photograph was 1100 TV lines/inch at a light level of the order 10^{-2} ft-candles. Target is underscanned.

Fig. 23 - Photographs of Display from E-II Ebicon.

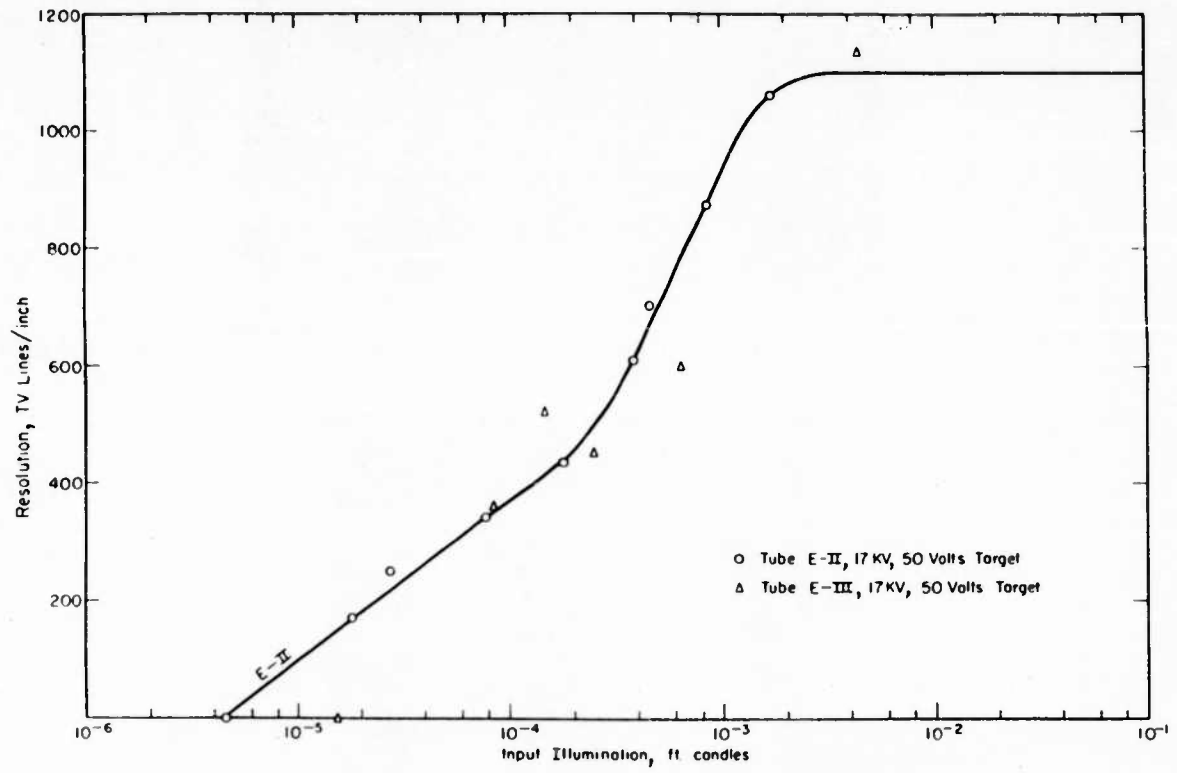


Fig 24 - Resolution vs input illumination for magnetically focused ebicons.

In response to a given photocathode current, the target current slowly would rise, at the same time as the image became increasingly visible.

When operated prior to insertion into the tube, the target had a gain of 450 at 20 KV and 50 volts on the target. As first measured in the tube at 50 volts target and at 16 KV on the image section, the gain was 187, for an input current corresponding to an illumination of 5.5×10^{-5} ft-candles. This value was obtained early in the life of the tube when the persistence was a few seconds, but as was pointed out, the target became slower after several days operation.

The target was relatively free from blemishes, had good contrast and normal storage characteristics. Except for the persistence, it was satisfactory in every visual characteristic. It is interesting to note that As_2S_2 targets, see E-IV, appear to be less susceptible to long term persistence effects.

Satisfactory focus could be achieved in a number of different modes. The tube was operated with a linear gradient from the photocathode to the last kovar flange before the target. The voltage on this last kovar could be adjusted over a wide range, keeping the photocathode-to-target voltage constant. Corresponding to this voltage on the last flange, a value of magnetic field could generally be found which would focus the image section. Since the scan and image sections were focused by the same magnetic coil, it was necessary to readjust the voltage on grid 3 of the scan section to achieve focus for the new magnetic field. Perhaps the best focus was obtained with 4.6 KV between photocathode and the last kovar flange when the photocathode-to-target voltage was 16 KV, but the advantage of this mode over other modes was slight. For these various modes, the required focus current varied from 80-150 gauss.

The resolution of the tube in TV lines/inch was of the order of 1100. Under optimum conditions it was about 1300 TV lines/inch in one direction. For a $7/16$ " diameter target, useful over 80% of its diameter, this yields about 450 TV lines.

The minification from photocathode to target was about 1.5. This gave a useful photocathode diameter of about 0.67 inches. It is evident that a larger area photocathode would result in proportionally low thresholds.

The general construction of the tube is shown in Fig. 25.

d. Tube E-III

The performance of tube E-III was similar to that of tube E-II. Resolution data are shown as a series of points on Fig. 25; these data show that the maximum resolution was somewhat higher than that of E-II, but that the tube was perhaps less sensitive at the low line numbers. This latter effect might be attributed to the 18 microampere per lumen photosurface which

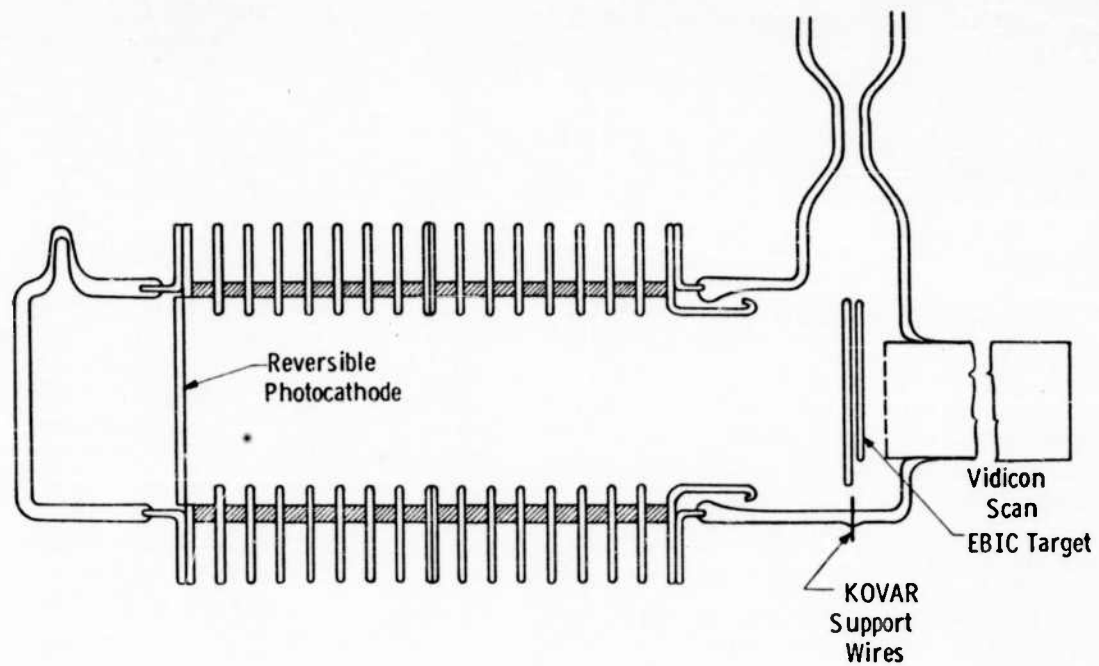


Fig. 25— Magnetically focused EBIC camera tube with vidicon scan

E-III had when constructed. Fourteen weeks later the response had dropped to 6.7 microamperes per lumen. Actual testing was done about nine weeks after manufacture.

This tube was similar to E-II also in that initially the target had a few seconds delay before either full gain or full erasure was realized. At a later testing however, the target was slower; for example, at a light level of 2.7×10^{-4} ft-candles, 35 seconds delay were required to realize a target gain of 100. At one of the threshold measurements, 100 seconds of viewing were necessary before the image became visible.

Although the tube was operable at least to 20 KV, there seemed to be little advantage in raising the photocathode-to-target voltage above 17 KV.

General imaging quality was good, being very similar to tube E-II. The general comments on imaging and focusing, described under E-II, also apply to this tube. As many as 9 shades of gray were seen. Resolution was the same in either of two perpendicular directions, and was reasonably uniform over the whole tube.

One section of the photocathode, about 20% of the entire area, had higher photosensitivity; this was noticeable particularly in photographs of the monitor, but not particularly objectionable in direct viewing. On the opposite edge of the target, there was an area which appeared bright when the high voltage was turned on. The target would then charge in a matter of a few seconds, and would operate normally. This charging effect was more noticeable than that which appears on the normal tube.

e. Tube E-IV

This tube, which made use of electrostatic focus on the image section and vidicon scan, was similar in structure to tube E-I except that the support structure of the target was divorced electrically from the last electrode of the image section lens system. This change in design permitted grounding the last electrode, thus allowing it to serve as a guard ring. This helped to minimize interference in the target signal circuit produced by high voltage instabilities in the image section. The revised structure also had the advantage of lowering the capacity of the target electrode.

The photoresponse as the tube came off exhaust was of the order of 30 ua/lumen. The initial performance of the tube was excellent. The tube operated stably to 14 KV, but little increase in threshold was noted as the target was increased from 10 KV to 14 KV.

The indications were that tube resolution was in excess of 400 TV lines. From rough tests the imaging threshold was estimated to be of the order of 10^{-6} ft-candles. The speed of response of the As_2S_2 target was excellent. Even after a 4 minute exposure at relatively high light level, very little trace of after image was noted.

Upon resuming testing after a 4 day interval, the initiation of gas discharges in the image section for voltages in excess of 500 volts was noted. The presence of gas in the tube was confirmed by a rise in photo-response to 48 ua/lumen. The tube getter was flashed and all glass-to-metal seals painted with glyptol. Photoresponse dropped to 10 ua/lumen and rose within a day to about 20 ua/lumen.

Unfortunately the high voltage stability of the tube was affected by the sequence of events. Two cold-emission bright spots could be observed on the monitor image of the target when the image section had 7 KV impressed across it. As voltage was raised, the general field emission background increased rapidly. At 10 KV high voltage flashing commenced.

The tube was rechecked after a 6 week interval. Photoresponse was still of the order of 20 ua/lumen, and the high voltage characteristics of the tube were observed to remain substantially unchanged. The threshold for imaging was determined to occur when 2.0×10^{-5} ft-candles were impressed on the photocathode for 10 KV on the image section and 36 target volts. This corresponds to an input current of about 8×10^{-12} amperes, and a signal current at target of about 7.5×10^{-10} amperes. On the demountable position thresholds below 10^{-13} amperes are frequently observed. Target gain was of the order of 100 for input currents between 8×10^{-12} and 2×10^{-10} amperes. However, the ability to observe threshold signals was very much affected by field emission. The speed of response of the target to both low and high signal levels remained excellent.

This target, which consisted of a .25 micron layer of Sb_2S_3 on a 1.4 micron layer of As_2S_3 evaporated over an aluminized self-supporting Al_2O_3 layer, originally had a target gain of about 600 at 30 target volts and 20 KV.

6) Conclusions

While the tubes constructed to date with vidicon scan have not reached the sensitivity theoretically, Ref. 16, attainable, they appear to be within a factor of 10 of the achievable value. The difference between tube performance and theory appears to be related to the signal-to-noise ratios at which the tubes will operate. Tests in the demountable vidicon scan position have indicated that the imaging threshold of present EBIC targets corresponds to target signal currents of the order of 2×10^{-10} amperes. According to these results, the targets will threshold at a signal-to-noise ratio of 0.1, as compared to signal-to-noise ratios somewhat less than .01 as determined in the background work involved in the derivations of Ref. 16. Further work is required to investigate the discrepancies involved.

It is believed that a better understanding of the factors involved in determining the electron absorptivity of scanned targets may prove fundamental to the developing of better targets of the EBIC and PC type.

Because of the problems involved in making reliable measurements in a demountable position, it is recommended that the test work on improving targets be conducted under more rigorous vacuum environments. In fact, it is necessary to also investigate the effect of subjecting the targets to atmospheric conditions, as is now the case. The properties of many targets are radically affected by exposure to the atmosphere, including the humidity conditions which prevail. Work on such targets cannot be performed without arranging to fabricate and test the targets in the same vacuum position in which they are fabricated.

Such a program would make it possible to fabricate the targets, test them, and then subject them to various controlled conditions, such as elevated temperatures, exposure to cesium, etc. Should targets be developed which are damaged by atmospheric exposure, the injection technique affords a convenient method for inserting them in tubes after fabrication, testing them, and selecting a suitable target.

LIST OF REFERENCES

1. Lempert and Klotzbaugh, "Research and Development of a Camera Tube for Night Viewing," Report No. 6, June 13, 1961, Signal Corps Contract DA-36-039 sc-87397.
2. Shockley, "Hot Electrons in Ge and Ohm's Law," Bell System Technical Journal 30, 779 (1951).
3. Ryder, "Mobility of Holes and Electrons in High Electric Fields," Physical Rev. 90, 766 (1953).
4. Weimer and Cope, "Photoconductivity in Amorphous Se," RCA Rev. 12, 314 (1951).
5. Forgue, Goodrich and Cope, "Properties of Photoconductivities, Principally Sb_2S_3 ," RCA Rev. 12, 335 (1951).
6. Ioffe and Ioffe, "Semiconductors in Strong Electric Fields," Journal of Physics of USSR, 2, 283 (1940).
7. Lampert, "Simplified Theory of Space-Charge Limited Currents in an Insulator With Traps," Phys. Rev. 103, 1648 (1956).
8. Smith and Rose, "Space Charge Limited Currents In Single Crystals of CdS," Phys. Rev. 97, 1531 (1955).
9. Hachenberg and Brauer, "Secondary Electron Emission from Solids," Advances in Electronics and Electron Physics, XI, p. 413 (1959) Academic Press.
10. Dekker, "Secondary Electron Emission," Solid State Physics 6, 251 (1958) Academic Press.
11. Haxby, "Secondary Emission From MgO Films and Crystals," Proceeding of 4th National Conference on Tube Techniques, 142, September 1958, New York University Press.
12. Jacobs and Dobischek, "Interaction of Slow Electrons and Surface Films of Ionic Crystals," Phys. Rev. 81, 1019 (1951).
13. Jacobs, Greenley, Gable, Ramsa, "Resonance Potentials in Thin Films of KCl," Phys. Rev. 106, 921 (1957).
14. Jacobs, Martin, and Brand, "Secondary Emission From Composite Surfaces," Phys. Rev. 85, 441 (1952).
15. Fredericks and Cook, "Interaction of Slow Electrons with Insulating Crystals," Phys. Rev. 121, 1693 (1961).
16. Lempert and Klotzbaugh, "Research and Development of a Camera Tube for Night Viewing," Signal Corps Contract DA36-039 sc-78920, Final Report, September 30, 1961.

DISTRIBUTION LIST
ASD Technical Report 61-657, Contract AF 33(616)-6496

Cys ACTIVITIES AT WPAFB

1 ASAPR (OTS Review)
1 ASAPR (Library)
3 ASAPT
2 ASRARS-1
10 ASRNET-2
10 ARX

OTHER DEPT. OF DEFENSE ACTIVITIES

Air Force

1 Commander
Rome Air Development Center
ATTN: RCSGA, Mr. Kesselman
Griffiss Air Force Base, New York

1 Commander
Air Force Special Weapons Center
ATTN: SWOI
Kirtland Air Force Base, New Mexico

1 Commander
Air Force Missile Test Center
ATTN: AFMTC Tech. Library MU-135
Patrick AFB Fla

1 Air University Library (7575)
Maxwell Air Force Base, Alabama

1 Commander
Rome Air Development Center
ATTN: RCSSL-1, Documents Library
Griffiss Air Force Base, New York

1 Commander
Air Proving Ground Center
ATTN: PGTRI
Eglin Air Force Base, Florida

1 Commander
Ballistic Systems Division
Air Force Unit Post Office
ATTN: WDTG
Los Angeles 45, California

1 Commander
Air Force Missile Development Center
ATTN: MDCRT-1
Holloman Air Force Base, New Mexico

Cys Air Force (Cont'd)

1 Commander
Electronic Systems Division
L. G. Hanscom Field
Bedford, Massachusetts

1 Commander
Space Systems Division
Air Force Unit Post Office
Los Angeles 45, California

Navy

1 Chief
Bureau of Ships
ATTN: Mrs. F. R. Darne, Code 691A
Washington 25, D. C.

1 Chief
Naval Research Laboratory
Bldg. 33, Room 105
Washington 25, D. C.

1 Naval Ordnance Test Station
ATTN: Mr. J. Rughe
1207 Michelson Laboratory
China Lake, California

Army

1 Commanding General
U. S. Army Engineer Research and
Development Laboratory
ATTN: Warfare Vision Branch
Ft. Belvoir, Virginia

1 Commanding Officer
U. S. Army Signal Research and
Development Laboratory
ATTN: SIGFM/EL-PRC
Ft. Monmouth, New Jersey

1 Commanding Officer
U. S. Army Electronic Proving Ground
ATTN: Combat Area Surveillance Department
Ft. Huachuca, Arizona

1 Commanding General
Frankford Arsenal
ATTN: Dr. R. L. Chwelow, 1130
Philadelphia 37, Pennsylvania

DISTRIBUTION LIST (Cont'd)
ASD Technical Report 61-657, Contract AF 33(616)-6496

Cys OTHER U.S. GOVERNMENT
 AGENCIES

- 30 Armed Services Technical Information
 Agency
 ATTN: TIPCRR
 Arlington Hall Station
 Arlington 12, Virginia
- 100 Office of Technical Services
 Department of Commerce
 Washington 25, D. C.
- 4 Advisory Group on Electronic Devices
 ATTN:: Secretary, Working Group on
 Special Devices
 346 Broadway, 8th floor
 New York 13, New York

NON-GOVERNMENT INDIVIDUALS
AND ORGANIZATIONS

- 1 The Rand Corporation
 ATTN: Librarian
 1700 Main Street
 Santa Monica, California
- 3 Radio Corporation of America
 ATTN: Mr. G. W. Kimball
 224 North Wilkinson Street
 Dayton 2, Ohio
- 1 General Electric Company
 Cathode Ray Tube Department
 ATTN: Dr. P. Wargo
 Electronics Park
 Syracuse, New York
- 1 University of Minnesota
 Institute of Technology
 Department of Electrical Engineering
 ATTN: Dr. W. G. Shepherd
 Minneapolis, Minnesota
- 1 Massachusetts Institute of Technology
 Lincoln Laboratory
 ATTN: Library
 P. O. Box 73
 Lexington 73, Massachusetts

Aeronautical Systems Division, Dir/Avionics,
Electronic Technology Lab, Wright-Patterson
AFB, Ohio.

Rpt Nr ASD-TR-61-657. RESEARCH ON
ELECTRON BOMBARDMENT INDUCED
CONDUCTIVITY TARGETS IN CAMERA
TUBES. Final report, Apr 62, 64p. incl
illus., tables, 16 refs.

Unclassified Report

An analysis of scan parameters as they affect
the performance of electron bombardment
induced conductivity (EBIC) targets is pre-
sented. The conclusion is reached that the
secondary emission characteristic of the
target surface is an extremely important
parameter in camera tubes of the photo-

(over)

conductivity and EBIC types. Evidence that
the electron absorptivity of the target for low
voltage electrons is affected by the degree of
induced excitation is presented. Results of
an investigation of different EBIC target
materials are reviewed. The fabrication of
experimental EBIC tubes having electro-
static and magnetic focused image sections
is described. Test results to date are
discussed.

1. Electron tubes
2. Camera tubes
3. Electron bombardment
induced conductivity

I. AFSC Project 4156,
Task 415605
II. Contract AF33(616)-
6496

III. Westinghouse Re-
search Lab.,
Pittsburgh, Pa.

IV. J. Lempert and
G. Klotzbaugh

V. In ASTIA collection
VI. Avail fr OTS

Aeronautical Systems Division, Dir/Avionics,
Electronic Technology Lab, Wright-Patterson
AFB, Ohio.

Rpt Nr ASD-TR-61-657. RESEARCH ON
ELECTRON BOMBARDMENT INDUCED
CONDUCTIVITY TARGETS IN CAMERA
TUBES. Final report, Apr 62, 64p. incl
illus., tables, 16 refs.

Unclassified Report

An analysis of scan parameters as they affect
the performance of electron bombardment
induced conductivity (EBIC) targets is pre-
sented. The conclusion is reached that the
secondary emission characteristic of the
target surface is an extremely important
parameter in camera tubes of the photo-

(over)

conductivity and EBIC types. Evidence that
the electron absorptivity of the target for low
voltage electrons is affected by the degree of
induced excitation is presented. Results of
an investigation of different EBIC target
materials are reviewed. The fabrication of
experimental EBIC tubes having electro-
static and magnetic focused image sections
is described. Test results to date are
discussed.

Aeronautical Systems Division, Dir/Avionics,
Electronic Technology Lab, Wright-Patterson
AFB, Ohio.
Rpt Nr ASD-TR-61-657. RESEARCH ON
ELECTRON BOMBARDMENT INDUCED
CONDUCTIVITY TARGETS IN CAMERA
TUBES. Final report, Apr 62, 64p. incl
illus., tables, 16 refs.

Unclassified Report
An analysis of scan parameters as they affect
the performance of electron bombardment
induced conductivity (EBIC) targets is pre-
sented. The conclusion is reached that the
secondary emission characteristic of the
target surface is an extremely important
parameter in camera tubes of the photo-

(over)

conductivity and EBIC types. Evidence that
the electron absorptivity of the target for low
voltage electrons is affected by the degree of
induced excitation is presented. Results of
an investigation of different EBIC target
materials are reviewed. The fabrication of
experimental EBIC tubes having electro-
static and magnetic focused image sections
is described. Test results to date are
discussed.

1. Electron tubes
2. Camera tubes
3. Electron bombardment
induced conductivity
I. AFSC Project 4156,
Task 415605
II. Contract AF33(616)-
6496

III. Westinghouse Re-
search Lab.,
Pittsburgh, Pa.
IV. J. Lempert and
G. Klotzbaugh
V. In ASTIA collection
VI. Aval fr OTS

Aeronautical Systems Division, Dir/Avionics,
Electronic Technology Lab, Wright-Patterson
AFB, Ohio.
Rpt Nr ASD-TR-61-657. RESEARCH ON
ELECTRON BOMBARDMENT INDUCED
CONDUCTIVITY TARGETS IN CAMERA
TUBES. Final report, Apr 62, 64p. incl
illus., tables, 16 refs.

Unclassified Report
An analysis of scan parameters as they affect
the performance of electron bombardment
induced conductivity (EBIC) targets is pre-
sented. The conclusion is reached that the
secondary emission characteristic of the
target surface is an extremely important
parameter in camera tubes of the photo-

(over)

conductivity and EBIC types. Evidence that
the electron absorptivity of the target for low
voltage electrons is affected by the degree of
induced excitation is presented. Results of
an investigation of different EBIC target
materials are reviewed. The fabrication of
experimental EBIC tubes having electro-
static and magnetic focused image sections
is described. Test results to date are
discussed.

1. Electron tubes
 2. Camera tubes
 3. Electron bombardment induced conductivity
- I. AFSC Project 4156, Task 415605
 - II. Contract AF33(616)-6496
 - III. Westinghouse Research Lab., Pittsburgh, Pa.
 - IV. J. Lempert and G. Klotzbaugh
 - V. In ASTIA collection
 - VI. Avail fr OTS

Aeronautical Systems Division, Dir/Avionics, Electronic Technology Lab, Wright-Patterson AFB, Ohio.
 Rpt Nr ASD-TR-61-657. RESEARCH ON ELECTRON BOMBARDMENT INDUCED CONDUCTIVITY TARGETS IN CAMERA TUBES. Final report, Apr 62, 64p. incl illus., tables, 16 refs.

Unclassified Report
 An analysis of scan parameters as they affect the performance of electron bombardment induced conductivity (EBIC) targets is presented. The conclusion is reached that the secondary emission characteristic of the target surface is an extremely important parameter in camera tubes of the photo-

(over)

conductivity and EBIC types. Evidence that the electron absorptivity of the target for low voltage electrons is affected by the degree of induced excitation is presented. Results of an investigation of different EBIC target materials are reviewed. The fabrication of experimental EBIC tubes having electrostatic and magnetic focused image sections is described. Test results to date are discussed.

1. Electron tubes
 2. Camera tubes
 3. Electron bombardment induced conductivity
- I. AFSC Project 4156, Task 415605
 - II. Contract AF33(616)-6496
 - III. Westinghouse Research Lab., Pittsburgh, Pa.
 - IV. J. Lempert and G. Klotzbaugh
 - V. In ASTIA collection
 - VI. Avail fr OTS

Aeronautical Systems Division, Dir/Avionics, Electronic Technology Lab, Wright-Patterson AFB, Ohio.
 Rpt Nr ASD-TR-61-657. RESEARCH ON ELECTRON BOMBARDMENT INDUCED CONDUCTIVITY TARGETS IN CAMERA TUBES. Final report, Apr 62, 64p. incl illus., tables, 16 refs.

Unclassified Report
 An analysis of scan parameters as they affect the performance of electron bombardment induced conductivity (EBIC) targets is presented. The conclusion is reached that the secondary emission characteristic of the target surface is an extremely important parameter in camera tubes of the photo-

(over)

conductivity and EBIC types. Evidence that the electron absorptivity of the target for low voltage electrons is affected by the degree of induced excitation is presented. Results of an investigation of different EBIC target materials are reviewed. The fabrication of experimental EBIC tubes having electrostatic and magnetic focused image sections is described. Test results to date are discussed.

Aeronautical Systems Division, Dir/Avionics,
Electronic Technology Lab, Wright-Patterson
AFB, Ohio.

Rpt Nr ASD-TR-61-657. RESEARCH ON
ELECTRON BOMBARDMENT INDUCED
CONDUCTIVITY TARGETS IN CAMERA
TUBES. Final report, Apr 62, 64p. incl
illus., tables, 16 refs.

Unclassified Report
An analysis of scan parameters as they affect
the performance of electron bombardment
induced conductivity (EBIC) targets is pre-
sented. The conclusion is reached that the
secondary emission characteristic of the
target surface is an extremely important
parameter in camera tubes of the photo-

(over)

conductivity and EBIC types. Evidence that
the electron absorptivity of the target for low
voltage electrons is affected by the degree of
induced excitation is presented. Results of
an investigation of different EBIC target
materials are reviewed. The fabrication of
experimental EBIC tubes having electro-
static and magnetic focused image sections
is described. Test results to date are
discussed.

1. Electron tubes
2. Camera tubes
3. Electron bombardment
induced conductivity

I. AFSC Project 4156,
Task 415605
II. Contract AF33(616)-
6496

- III. Westinghouse Re-
search Lab.,
Pittsburgh, Pa.
- IV. J. Lempert and
G. Klotzbaugh
- V. In ASTIA collection
- VI. Avail fr OTS

Aeronautical Systems Division, Dir/Avionics,
Electronic Technology Lab, Wright-Patterson
AFB, Ohio.

Rpt Nr ASD-TR-61-657. RESEARCH ON
ELECTRON BOMBARDMENT INDUCED
CONDUCTIVITY TARGETS IN CAMERA
TUBES. Final report, Apr 62, 64p. incl
illus., tables, 16 refs.

Unclassified Report
An analysis of scan parameters as they affect
the performance of electron bombardment
induced conductivity (EBIC) targets is pre-
sented. The conclusion is reached that the
secondary emission characteristic of the
target surface is an extremely important
parameter in camera tubes of the photo-

(over)

conductivity and EBIC types. Evidence that
the electron absorptivity of the target for low
voltage electrons is affected by the degree of
induced excitation is presented. Results of
an investigation of different EBIC target
materials are reviewed. The fabrication of
experimental EBIC tubes having electro-
static and magnetic focused image sections
is described. Test results to date are
discussed.